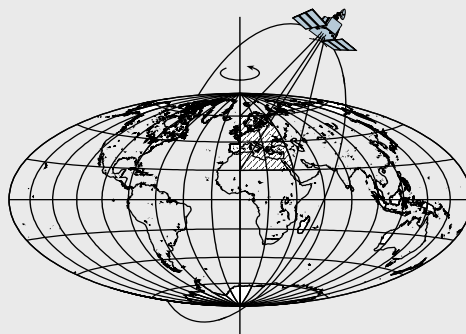


A COMPARATIVE OVERVIEW OF GEOPHYSICAL METHODS

by

Kamil Erkan



Report No. 488

Geodetic Science and Surveying

The Ohio State University
Columbus, Ohio 43210

September 2008

A Comparative Overview of Geophysical Methods

Kamil Erkan

Division of Geodesy and Geospatial Science
School of Earth Sciences
The Ohio State University, Columbus, OH 43210
erkan.1@osu.edu

Abstract:

The shallow subsurface structure of the Earth is important to understand for many economic and safety reasons. The problem is usually difficult due to complexity of the earth's subsurface processes especially near the surface. A number of geophysical methods are used for this purpose using different physical characteristics of the Earth materials. A particular geophysical method illuminates part of the problem, but a reliable solution can only be found by combining results of different methods. In order to synthesize information from different geophysical methods, it is important to understand their similarities and differences. The aim of this study is to correlate the basic principles of geophysical methods side-by-side starting from fundamental equations. This study reveals that many analogies exist among these methods both in their mathematical formulation, and sometimes, in ways they are used in the geophysical applications.

Acknowledgements:

I wish to thank Dr. Christopher Jekeli for critically reviewing the manuscript. This report was prepared with support from the Air Force Research Laboratory, under contract FA8718-07-C-0021.

Table of Contents

Part I Introduction

1. Overview of geophysical methods, *1*
2. Practical methods in geophysical prospecting, *2*

Part II Mathematical Formulations

3. Fundamental properties of sources, *6*
4. Some mathematical identities, *6*
5. Fields due to distance sources, *9*
 - a. Static fields due to point sources, *9*
 - b. Static fields of volumetric sources, *12*
 - c. Green's functions for static fields, *15*
 - d. Maxwell equations in free space, *16*
6. Fields in sourced media, *18*
 - a. Electric and magnetic polarization in sourced media, *18*
 - b. Maxwell equations in sourced media, *20*
 - c. Seismic fields, *25*
7. Comparison of the mathematical formulations, *27*

Part III Present Applications of the Geophysical Methods

8. Physical properties of earth materials, *29*
9. Static field methods, *30*
 - a. Gravimetry, *30*
 - b. Magnetometry, *35*
 - c. MMR method, *41*
 - d. DC resistivity, *42*
10. Diffusive field methods, *46*
 - a. MT method, *46*
 - b. EM/TEM induction method, *48*
 - c. IP method, *50*
 - d. SASW method, *51*
11. Transient field methods, *52*
 - a. Seismic refraction method, *53*
 - b. GPR method, *53*
 - c. Seismic reflection method, *56*
12. Discussion, *56*
 - a. Comparison of electrical methods, *57*
 - b. Relevance of methods for void detection, *58*

References

Appendix A

Introduction

1. Overview of Geophysical methods

Geophysics is a branch of the Earth sciences which aims to understand the Earth using the methods of physics. Its application areas are generally related to understanding the subsurface structure of the Earth which is important for both scientific and economical reasons. A general classification of the methods currently used in the geophysical arena and some of their basic characteristics are given in Table 1.1.

Table 1.1 General classifications of geophysical methods

Geophysical Method	Main sources of the fields	Depths of application	Main Application areas	Survey methods
Gravity	- Natural: (gravitational masses of rocks)	Entire of the Earth	Mining Hydrology Plate tectonics Mantle dynamics Core dynamics	Ground Airborne Spaceborne
Magnetostatic	- Natural (Outer Core convection; solar storms; magnetization of near-surface rocks)	0-20 km 3000-6450 km	Basin analysis Plate tectonics Paleo-tectonics Core dynamics	Ground Airborne Spaceborne
DC resistivity	- Artificial (electric current sources)	0-0.1 km	Hydrology Ore mining	Ground
Magnetotelluric	- Natural (Ionospheric events)	0-150 km	Hydrology Plate tectonics	Ground
Electromagnetic induction	- Artificial (electromagnetic induction)	0-10 km	Geologic mapping Ore mining Metal detection	Ground Airborne
Electromagnetic radiation (GPR)	- Artificial (electromagnetic radiation)	0-0.05 km	Geotechnology Hydrology Archeology	Ground Airborne
Seismic reflection	- Artificial (explosives; falling loads)	0-10 km	Basin analysis	Ground
Seismic refraction	- Artificial (explosives; falling loads)	0-150 km	Basin analysis Crustal studies Plate tectonics	Ground
Earthquake seismology	- Natural (earthquakes in the Crust)	10-6450 km	Plate tectonics Mantle dynamics Core dynamics	Ground
Heat flow	- Natural (radioactivity of rocks; secular heat of the Earth)	0.1-120 km	Crustal rheology Plate tectonics Mantle rheology	Ground

Geophysics uses certain instruments to detect one property of the physical field related to the Earth, and then uses this information to obtain information about the subsurface. However, not all the geophysical tools are enough to resolve any part of the Earth. Some methods are more powerful in the shallow parts (e.g. reflection seismology and electromagnetic) whereas others can retrieve information from the very deepest parts of the Earth (e.g. gravity and earthquake seismology).

In geophysics one can take advantage of the Earth's natural fields (passive source) or can generate artificial fields (active source) (Table 1.1). The natural fields can originate from a combination of sources including those of the specific target in the Earth that is being investigated. So, one has to eliminate the contribution from all of other sources in order to get a useful signal. One advantage of natural sources is that they do not require an additional deployment to generate the field. On the other hand, the main advantage of the artificial fields is that the source parameters can be predetermined and can be used to eliminate the noise and obtain a strong signal.

Some of the fields may originate from deeper parts of the Earth (such as gravity, magnetic) or interact in deeper parts of the Earth (such as earthquake waves) that can be used to understand the gross structure of the Earth; and they are the subjects of theoretical geophysics. On the other hand, shallow field methods are very important for economical purposes. In Table 1.1, all except the last two methods are routinely used in near-surface geophysical applications. For practical purposes, the following discussion only deals with the methods used in near-surface applications.

2. Practical methods in geophysical prospecting

In geophysical prospecting, the purpose is to get the knowledge of the shallow (i.e. <10 km) subsurface using various physical tools. A very general listing of the methods with some of their characteristics is given in Table 2.1.

Gravity methods:

Earth's gravity field in first order approximation is that of an oblate spheroid. However, measurement of gravitational acceleration at the same altitude shows considerable variations. The wave length of the variations is related to the depth of the density within the Earth. A very large scale variation (~1000 km) can be related to lateral heterogeneity of the Earth's crust and mantle, and to the thermal and compositional variations. At very small wavelengths (<1 km), the change in the gravity field can be attributed to very shallow anomalies, such as a sulfide body or a subsurface void, as well as the general topography of the surface.

Technological improvements in the design and sensitivity of measurements devices in gravity offer continuously widening areas of applications. One of the newly emerging of gravitational methods is the highly sensitive measurements of the time variable gravity, which allow applications both in the space and time domains (4-D gravity). Very sensitive satellite gravimetry surveys available for monitoring the global field allow monitoring of mass movements associated with hydrology and large scale glaciers and ice sheets, which is an important issue in the study of global climate change.

Magnetic methods:

The Earth has a finite magnetic field which can be measured on the surface (60000 nT at the poles and 25000 nT at the equator). This field appears to be generated by the convection of the

liquid iron Outer Core. On the Earth's surface, 90% of the field can be attributed to that of a dipole oriented along the polar axis (with about 11° deviation from the geographic pole). Part of this dipole approximation can be attributed to the rapid decay of the higher order moments of the magnetic field in passing through great distances of the mantle. So, the total magnetic field ends up being a relatively smooth dipole field on the surface of the Earth.

Table 2.1 Methods used in geophysical prospecting and their characteristic properties

Geophysical Method	Measured property	Investigated physical property	Main practical obstacle
Gravimetry and Gradiometry	Acceleration vector and its gradient	- Density contrast	Relatively small variations in densities of rocks
Magnetostatic	Magnetic field vector	- Magnetic permeability	Low magnetic strength of rocks
DC resistivity	Electric potential change	- Resistivity	Low depth of penetration due to resistivity of rocks
Magnetotelluric	Amplitudes of electromagnetic fields	- Resistivity	Fast attenuation due to conductivity of rocks
Electromagnetic induction	Phase/amplitude change of the magnetic field	- Resistivity - Dielectric permittivity	Fast attenuation due to conductivity of rocks
Electromagnetic radiation (GPR)	Electromagnetic travel time	- Contrasts in electromagnetic wave impedance	Fast attenuation due to conductivity of rocks
Seismic refraction	Seismic travel time	- Seismic velocity	Seismic wave attenuation
Seismic reflection	Seismic travel time	- Contrasts in acoustic wave impedance	Seismic wave attenuation

Earth's magnetic field acts like a natural source that illuminates below the surface of the Earth. That is, the external magnetic field induces an additional magnetic field inside the rocks which can be measured on the surface of the Earth as an anomaly. Since, the magnitude of the induction depends on the rock type; the anomalous field becomes a proxy to obtain information about the subsurface structure.

Some rocks have natural magnetization (magnets) even in the absence of an external magnetic field (remnant magnetization). All rocks lose their magnetic properties beyond a certain temperature called the Curie temperature (500-600 C° for peridotite). Remnant magnetization has some implications in the study of the Earth's lithosphere. On the beneficial side, as molten rocks cool on their way up to the Earth's surface, they become magnetized in the direction of the Earth's ambient field at the time of cooling. Then the magnetic properties of these rocks act like a "magnetic record" in geologic time, which can eventually be used to understand the past plate motions. Especially, this phenomenon leads to the formation of an outstanding magnetic pattern in the oceans due to the highly magnetic content of the oceanic crust (dominantly in basalt). On the down side, the remnant magnetization of rocks can sometimes complicate the interpretation in continental areas if the direction of remnant magnetization is unknown due to complicated past tectonic activities.

Electric and electromagnetic methods:

Unlike as a magnetic field source, the Earth does not generate a terrestrial electric field that can be measured on the surface (all the natural electric fields measured on the surface are either from solar storms or due to atmospheric events). However, in shallow parts of the Earth (1-100 km, depending on the wavelength) electric fields do exist due to the penetration of electromagnetic waves generated in the atmosphere. These waves also accompany naturally occurring electric conduction within the Earth (telluric currents). Alternatively, the electric field can be generated by a man-made electric source (active source). In either case, these electric fields enter the Earth and interact with the medium, and return the knowledge of the medium through which they pass. However, this interaction can be complicated compared to the interaction of the gravity and magnetic fields, due to the existence of free electric sources inside the Earth (discussed below).

In direct current (DC resistivity) methods, most of the response of the rocks is related to the electrical resistivity of the rocks, which can be used to understand the subsurface structure. However, most of the Earth materials have a range of resistivities similar to each other with the exception of metallic ores and water which are very good conductors (and, the rocks with high clay content, which is a highly conductive mineral). Due to this contrast, DC methods are largely useful for studying metal ores and groundwater.

In electromagnetic induction methods, low frequency (quasi-stationary) fields are used to obtain penetration into the Earth. Due to dissipation of electric energy (mainly into heat) due to finite electric conductivity of rocks, artificial source methods have limited depth of penetration. However, powerful and long wavelength electromagnetic signals can be generated by atmospheric sources, which can penetrate 100-150 km into the Earth, and constitute the only useful applications of the electric methods in theoretical studies (the magnetotelluric method). The magnetotelluric (MT) method is also useful for shallow applications using higher frequency fields and specifically called the audio-magnetotelluric (AMT) method.

High frequency electromagnetic fields (radiation form) are also used for very shallow applications (< 50 m), which takes advantage of the contrasts in dielectric properties of rocks. The method is known as ground penetrating radar (GPR) in the geophysical nomenclature as it has the same basic principles of conventional radar systems. GPR method uses the contrasts of electrical properties between mediums rather than the internal electric properties of a medium. By this characteristic, the method is in fact an imaging method, similar to the method of seismic reflection (discussed below). As in the case of electromagnetic induction, the depth of penetration with GPR is also limited by the finite electric conductivity of the rocks. GPR is particularly used for shallow applications due to limited depth of penetration of high frequency electromagnetic waves.

Rocks are weak semiconductors with relatively similar resistivities and dielectric constants. On the other hand, water (occupying the pore spaces inside the rocks in the shallow subsurface) has relatively much higher dielectric constant and lower resistivity, and almost entirely determines electric conductivity and permittivity of the bulk medium. As a result of this fact, the measured signals in electric and electromagnetic methods carry mostly the information about the hydrologic state of the subsurface structure (i.e. porosity of the rocks), unless the electric properties of the target are distinctly different from the background (such as ores), or the medium is dry. If a study is not intended for hydrological purposes, the electric and electromagnetic methods are best for low electric conductivity environments.

Seismic methods:

Seismic methods started to develop after realization that earthquakes cause shear and pressure waves traveling inside the earth (mid-18th century). Seismic waves are generated by external forces acting on the molecular crystals that constitute the rocks, which behave like molecular springs that lead to the creation of waves. The wavelength and amplitude of seismic waves are related to the size of their source. In the case of earthquakes, forces are generated by motions of the tectonic plates that result in large wavelengths and amplitudes of seismic waves which can travel great distances within the Earth and can still be measured as they return to the Earth surface. The largest seismic waves are associated by the free oscillations of the Earth that form after great earthquakes, which have frequencies of ~ 1 mHz and wavelengths $\sim 10,000$ km. These events are used to understand the gross structure of the Earth (e.g. bulk density and viscosity). Alternatively, artificial earthquakes generated by explosives near the Earth's surface can yield information about the subsurface structures. Although they are much smaller in amplitude and wavelength, ingenious deployment methods (both refraction and reflection methods) can lead to greatly detailed information for the shallower parts below the Earth's surface.

Mathematical Formulations

3. Fundamental properties of sources

In Newtonian physics, all the forces that can act on a body with mass m , electric charge q , and velocity \mathbf{v} can be stated by the Lorentz equation with the addition of the gravitational term as

$$\mathbf{F} = m \cdot \mathbf{g} + q \cdot \mathbf{E} + q \cdot \mathbf{v} \times \mathbf{B}$$

$$\mathbf{g} = (g_x, g_y, g_z)$$

$$\mathbf{E} = (E_x, E_y, E_z)$$

$$\mathbf{B} = (B_x, B_y, B_z)$$

In this equation, the vectors $\{\mathbf{g}, \mathbf{E}, \mathbf{B}\}$ are called the force fields. It is evident that \mathbf{E} and \mathbf{B} are fundamentally related to each other as they both act on the same charge q . In fact, although theoretically natural magnetic monopoles can exist, they haven't been observed so far; so all the magnetic fields observed in nature are assumed to be created by electric sources. As it will be shown below, the smallest magnetic source can be represented by a circulating current loop which generates a dipole magnetic field, and shows all the properties of a "real" magnetic dipole. So, it can conveniently be assumed that real magnetic dipoles exist anywhere outside of the source which causes the dipole magnetic field.

As opposed to gravity, which is represented by monopoles, electric and magnetic sources can have both positive and negative charges (Table 3.1). As a result of this, the interaction of electric and magnetic fields inside a medium with sources can be complicated as they polarize the medium passing through (discussed below).

Interaction of the electric field inside a medium is even more complicated than the magnetic field since an external electric field can mobilize the free electric charges of atoms, which leads to conduction. On the other hand, interaction of the magnetic field inside the Earth does not lead to such mobilization as no free magnetic sources exist. From a practical perspective, magnetic fields generated by magnetized bodies (after the polarization is added) are analogous to gravity fields which are generated by stationary masses, with the exception that the gravity sources are scalar and the magnetic sources are directional (i.e. direction of magnetic polarization).

Table 3.1 Basic properties of sources of force fields

Field	Type	Polarization	Conduction
Gravity	Scalar	No	No
Magnetic	Vector	Yes	No
Electric	Scalar/vector	Yes	Yes

4. Some mathematical identities

Definition of a conservative field:

Any of following four statements proves that a force field is *conservative*. Validity of any one also validates the other three statements (Riley et al., 1997).

- i. The integral $\int_a^b \mathbf{F} \cdot d\mathbf{r}$ is independent of the path taken between points a and b .
- ii. There exists a scalar function U , which is related to the force field by $\mathbf{F} = \nabla U$.
- iii. The force field is irrotational i.e. $\nabla \times \mathbf{F} = 0$.
- iv. $\mathbf{F} \cdot d\mathbf{r}$ is an exact differential.

In the discussion below, the following are useful vector identities:

$$\nabla \times (\nabla U) = \mathbf{0}, \text{ i.e. the curl of the gradient is zero.} \quad (4.1)$$

$$\nabla \cdot (\nabla \times \mathbf{F}) = 0, \text{ i.e. the divergence of the curl is zero.} \quad (4.2)$$

$$\nabla^2 \mathbf{F} = \nabla(\nabla \cdot \mathbf{F}) - \nabla \times (\nabla \times \mathbf{F}) \quad (\text{Laplacian of a vector field}) \quad (4.3)$$

$$\nabla^2 U = \nabla \cdot (\nabla U) \quad (\text{Laplacian of a scalar field}) \quad (4.4)$$

Some Integral Formulae:

Some useful integral formulae are given in this section without their derivations. The formal derivations may be found in Baranov (1975).

Divergence Theorem: Let \mathbf{F} be any vector field and v an arbitrary volume with the surface area S . Then the divergence theorem states that

$$\int_v \nabla \mathbf{F} \cdot dv = \int_S \mathbf{F} \cdot \mathbf{n} \cdot dS \quad (4.5)$$

Here the vector \mathbf{n} is the unit normal vector on the surface, conventionally pointing outside of the volume v .

Green's Theorem: Defining two scalar fields U and V provided that their first and second derivatives exist, Green's theorem states that

$$\int_v (U \cdot \nabla^2 V - V \cdot \nabla^2 U) dv = \int_S \left(U \cdot \frac{dV}{dn} - V \frac{dU}{dn} \right) dS \quad (4.6)$$

In fact, Green's theorem is a consequence of the divergence theorem, and can be derived from it by defining a force field that is the difference,

$$\mathbf{F} = U \nabla V - V \nabla U$$

where U and V are scalar functions.

Gauss's Theorem: If we set $V=1$ in Green's theorem (4.6), then we get Gauss's theorem.

$$\int_v \nabla^2 U \cdot dv = \int_S \frac{dU}{dn} dS \quad (4.7)$$

For conservative fields, if we make the substitution of $\mathbf{F} = -\nabla U$, which implies that $\frac{dU}{dn} = -\mathbf{n} \cdot \mathbf{F}$, Gauss's theorem can also be stated in terms of the force field as

$$\int_v \nabla \cdot \mathbf{F} \cdot dv = \int_S \mathbf{n} \cdot \mathbf{F} dS \quad (4.8)$$

which is identical to the divergence theorem (4.5).

Gradient of distance and reciprocal distance:

Let's define a distance vector by $\mathbf{r} = (x, y, z)$ in three-dimensional space whose magnitude and unit vector are $r = |\mathbf{r}|$ and $\bar{\mathbf{r}} = \frac{\mathbf{r}}{r}$ respectively. The following relations hold (Baranov, 1975):

$$\nabla r = \bar{\mathbf{r}} \quad (4.9)$$

$$\nabla \left(\frac{1}{r} \right) = -\frac{\bar{\mathbf{r}}}{r^2} \quad (4.10)$$

$$\nabla^2 \left(\frac{1}{r} \right) = -4\pi\delta(r) \quad (4.11)$$

where the Dirac delta function $\delta(r)$ is defined as

$$\int_{\infty} \delta(x, y, z) dv = 1 \quad (4.12)$$

and

$$\int_{\infty} F(x, y, z) \delta(x, y, z) dv = F(0,0,0) \quad (4.13)$$

Here, $F(x,y,z)$ is a continuous and bounded function in the entire space, and dv is an element of volume. A formal derivation of (4.11) is given in the Appendix A.

As a corollary, in physical applications, the density (ρ) of a point mass/charge (m) can be defined using the definition of the Dirac delta function in (4.13):

$$\int \rho(x, y, z) dv = m = \int m(x, y, z) \delta(r) dv \quad (4.14)$$

Then, one obtains

$$m(x, y, z) \delta(r) = \rho(x, y, z) \quad (4.15)$$

Green's function:

Let a scalar field $U(\mathbf{r})$ be the solution of a source distribution $f(\mathbf{r})$ such that

$$\Re U(\mathbf{r}) = f(\mathbf{r}) \quad (4.16)$$

where \Re is a linear partial differential operator describing the field.

Let's suppose that a function $G(\mathbf{r}, \mathbf{r}_0)$ exists such that

$$U(\mathbf{r}) = \int_{v_0} f(\mathbf{r}_0) G(\mathbf{r}, \mathbf{r}_0) dv_0 \quad (4.17)$$

where \mathbf{r} and \mathbf{r}_0 represent distance vectors for points in the field and inside the source, respectively (see Figure 5.3). If (4.17) is substituted into (4.16), then, according to (4.13), one obtains

$$\Re G(\mathbf{r}, \mathbf{r}_0) = \delta(\mathbf{r} - \mathbf{r}_0) \quad (4.18)$$

According to this formula, the Green's function can also be defined as the solution of (4.16) to a Dirac delta function source. Specifically, from (4.11) we have

$$G(\mathbf{r}, \mathbf{r}_0) = -\frac{1}{4\pi} \frac{1}{|\mathbf{r} - \mathbf{r}_0|}. \quad (4.19)$$

5. Fields due to distant sources

5.a Static fields due to point sources

Gravity:

The gravitational field \mathbf{g} of a point source with mass m at a distance \mathbf{r} (Figure 5.1) is represented by Newton's inverse square law

$$\mathbf{g} = -G \frac{m}{r^2} \hat{\mathbf{r}} \quad (5.1)$$

The minus sign is a convention to show that the force is opposite to the direction of the distance vector. Using identity (4.10), the field equation (5.1) can be written as

$$\mathbf{g} = -G \frac{m}{r^2} \hat{\mathbf{r}} = Gm \nabla \left(\frac{1}{r} \right) = \nabla \left(\frac{Gm}{r} \right) = \nabla U \quad (5.2)$$

Here the potential for the gravitation field is defined as

$$U(\mathbf{r}) = \frac{Gm}{r} \quad (5.3)$$

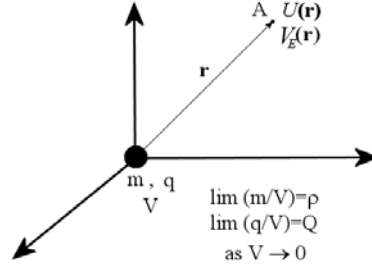


Figure 5.1 A point source in free space

If the Laplacian operator acts on (5.3), using (4.15) one obtains Poisson's equation for gravitation:

$$\nabla^2 U(\mathbf{r}) = \nabla^2 \left(\frac{Gm}{r} \right) = Gm \nabla^2 \left(\frac{1}{r} \right) = -Gm 4\pi \delta(\mathbf{r}) = -4\pi G \rho(\mathbf{r}) \quad (5.4)$$

Equation (5.4) is Poisson's equation of a point mass with density ρ . By the principle of superposition, Equation (5.4) can be generalized to represent any distribution of masses with different densities. In this case, $\rho(\mathbf{r})$ represents the density function of the arbitrary gravitational source. In free space, i.e. $\rho(\mathbf{r})=0$, Equation (5.4) reduces to Laplace equation for gravitational field, i.e.

$$\nabla^2 U(\mathbf{r}) = 0 \quad (5.5)$$

Electric point source:

The electric field \mathbf{E} due to a charge q is given by the Coulomb force acting on a unit charge and formulated as

$$\mathbf{E} = \frac{1}{4\pi\epsilon_0} \frac{q}{r^2} \mathbf{r} \quad (5.6)$$

Since alike charges repel each other no minus sign comes in Equation (5.6) by convention. Here, ϵ_0 is called the dielectric permittivity of free space. By the same procedure for the gravitational potential (5.4-5.5), the electric potential can be written as

$$V_E(\mathbf{r}) = \frac{1}{4\pi\epsilon_0} \frac{q}{r} \quad (5.7)$$

Note that the electric potential was defined as $\mathbf{E} = -\nabla V_E$. If the Laplacian operator acts on (5.7), one gets Poisson equation for electricity using (4.15):

$$\nabla^2 V_E(\mathbf{r}) = \frac{q}{4\pi\epsilon_0} \nabla^2 \left(\frac{1}{r} \right) = -\frac{q}{4\pi\epsilon_0} 4\pi\delta(\mathbf{r}) = -\frac{1}{\epsilon_0} Q(\mathbf{r}) \quad (5.8)$$

In free space, the potential field satisfies the Laplace equation:

$$\nabla^2 V_E(\mathbf{r}) = 0 \quad (5.9)$$

Electric dipole:

A dipole consists of two opposite charges with the same magnitude and separated by a distance $d = |\mathbf{d}|$ from each other (Figure 5.2), where the vector \mathbf{d} represent *the direction of polarization*.

In Figure 5.2, the potential at point A is a superposition of the contributions of the two point sources. Then, one can write

$$V_E(\mathbf{r}) = \frac{q}{4\pi\epsilon_0} \left(\frac{1}{r_+} - \frac{1}{r_-} \right) = \frac{q}{4\pi\epsilon_0} d \left[\frac{1}{d} \left(\frac{1}{r_+} - \frac{1}{r_-} \right) \right] \quad (5.10)$$

In Figure 5.2, if $d \ll r$, then the last term can be approximated as

$$\frac{1}{d} \left(\frac{1}{r_+} - \frac{1}{r_-} \right) \approx \frac{\partial}{\partial d} \left(\frac{1}{r} \right) \quad (5.11)$$

Then, the potential of an electric dipole becomes

$$V_E(\mathbf{r}) = \frac{qd}{4\pi\epsilon_0} \frac{\partial}{\partial d} \left(\frac{1}{r} \right) = \frac{p}{4\pi\epsilon_0} \nabla_d \left(\frac{1}{r} \right) \quad (5.12)$$

The term $\nabla_d(1/r)$ is the directional derivative of $1/r$ along d . In (5.12), we define *the electric dipole moment* $\mathbf{p} = q\mathbf{d}$, and its magnitude as $p = qd$. It can alternatively be defined as the scalar product of the vectors \mathbf{d} and $\nabla(1/r)$ (Figure 5.2). Then, one can also write

$$\mathbf{d} \cdot \nabla \left(\frac{1}{r} \right) = \frac{\partial}{\partial d} \left(\frac{1}{r} \right) = \frac{\partial}{\partial r} \left(\frac{1}{r} \right) \cos\theta = -\frac{1}{r^2} \cos\theta \quad (5.13)$$

where θ is as defined in Figure 5.2. Then (5.12) can also be written as

$$V_E(\mathbf{r}) = \frac{1}{4\pi\epsilon_0} \frac{p}{r^2} \cos\theta = -\frac{1}{4\pi\epsilon_0} \frac{\mathbf{p} \cdot \bar{\mathbf{r}}}{r^2} \quad (5.14)$$

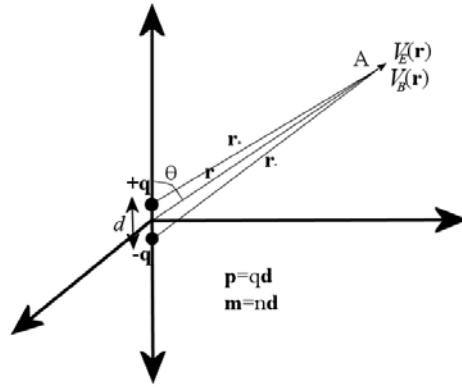


Figure 5.2 A dipole source in free space

Magnetic dipole:

We previously mentioned that the smallest magnetic source is a dipole, which shows the exact same properties of an electric dipole. Then, the same methodology of an electric dipole can be used to calculate the potential of a magnetic point dipole. If we replace the coefficient ϵ_0 by μ_0^{-1} in (5.14), and define the *magnetic dipole moment* \mathbf{m} analogous to the electric dipole moment, one can write the magnetic potential equation analogous to (5.14) as

$$V_B(r) = -\frac{\mu_0}{4\pi} \frac{\mathbf{m} \cdot \mathbf{r}}{r^2} \tag{5.15}$$

Here μ_0 is a scaling factor for the magnetic field and is called as *the magnetic permeability of free space*. If the magnetic dipole moment is defined as $\mathbf{m} = n\mathbf{d}$, n represents the strengths of the artificial magnetic poles, as \mathbf{d} is the same distance vector between the poles as in electric dipole (Figure 5.2).

By analogy to (5.12), the magnetic potential can also be written in the directional derivate form as

$$V_B(\mathbf{r}) = \frac{\mu_0 |\mathbf{m}|}{4\pi} \nabla_d \left(\frac{1}{r} \right) \tag{5.16}$$

We finally point out that unlike a monopole source whose potential decays by $1/r$ (see (5.3) and (5.7)), the potential of a dipole source decays by $1/r^2$ (see (5.14) and (5.16)).

5.b. Static fields of volumetric sources

If the density function defined in (4.15) is substituted into (4.14), one gets the following equations that relate the differential volumes to differential source strengths:

$$dm = \rho dv; \quad dq = Qdv; \quad dp = \mathbf{P}dv; \quad d\mathbf{m} = \mathbf{M}dv \tag{5.17}$$

Here, ρ and Q represent the mass and charge densities for monopoles. Above, we also defined two other density functions for dipole sources which are electric polarization (\mathbf{P} , generally named as *polarization*) and magnetic polarization (\mathbf{M} , generally named as *magnetization*). They are volume-normalized dipole moments of electric and magnetic dipole sources. Let's assume a body with a finite volume and charge distributions ($\rho, Q, \mathbf{P}, \mathbf{M}$) (Figure 5.3). In Figure 5.3, the vector \mathbf{r} represents a point in the field, whereas \mathbf{r}_0 represent a point in the source. The total volume can be assumed to be formed by individual small bodies (prisms) whose internal densities ($\rho, Q, \mathbf{P}, \mathbf{M}$) are constant. Then, one can take advantage of the principle of superposition, and define the total field as a summation. For infinitely small prisms, the summation takes the form of an integral.

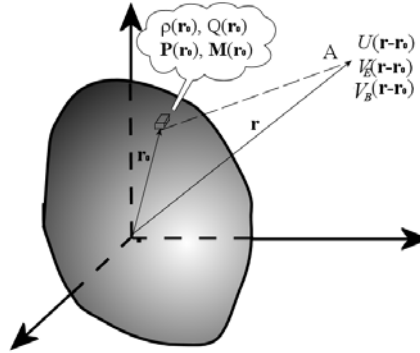


Figure 5.3 A volumetric source in free space

Gravitational field:

Using the principle of superposition, the total gravitational potential at a Point A in free space can be written using (5.3) as

$$U(\mathbf{r}) = \int_{v_0} \frac{Gdm(\mathbf{r}_0)}{|\mathbf{r} - \mathbf{r}_0|} = \int_{v_0} \frac{G\rho(\mathbf{r}_0)}{|\mathbf{r} - \mathbf{r}_0|} dv_0 = G \int_{v_0} \frac{\rho(\mathbf{r}_0)}{|\mathbf{r} - \mathbf{r}_0|} dv_0 \quad (5.18)$$

In the equation, dv_0 represents that the integral is taken over the sources only.

Electrostatic field:

Using (5.7), the total electric potential at Point A can be written as

$$V_E(\mathbf{r}) = \int_{v_0} \frac{1}{4\pi\epsilon_0} \frac{dq(\mathbf{r}_0)}{|\mathbf{r} - \mathbf{r}_0|} = \frac{1}{4\pi\epsilon_0} \int_{v_0} \frac{Q(\mathbf{r}_0)}{|\mathbf{r} - \mathbf{r}_0|} dv_0 \quad (5.19)$$

For a body with electric dipole distribution, using (5.14), the total potential becomes

$$V_E(\mathbf{r}) = - \int_{v_0} \frac{1}{4\pi\epsilon_0} \frac{d\mathbf{p}(\mathbf{r}_0) \cdot \overline{(\mathbf{r} - \mathbf{r}_0)}}{|\mathbf{r} - \mathbf{r}_0|^2} = - \frac{1}{4\pi\epsilon_0} \int_{v_0} \mathbf{P}(\mathbf{r}_0) \cdot \frac{\overline{(\mathbf{r} - \mathbf{r}_0)}}{|\mathbf{r} - \mathbf{r}_0|^2} dv_0 \quad (5.20)$$

Using (4.10), the last integral can also be stated as

$$V_E(\mathbf{r}) = \frac{1}{4\pi\epsilon_0} \int_{v_0} \mathbf{P}(\mathbf{r}_0) \cdot \nabla \left(\frac{1}{|\mathbf{r} - \mathbf{r}_0|} \right) dv_0 \quad (5.21)$$

Magnetostatic field:

Similar to the derivations for the electric field, one can calculate the magnetic potential due to a volume of magnetic dipoles by integrating (5.15) over the volume

$$V_B(\mathbf{r}) = - \int_{v_0} \frac{\mu_0}{4\pi} \frac{d\mathbf{m}(\mathbf{r}_0) \cdot (\mathbf{r} - \mathbf{r}_0)}{|\mathbf{r} - \mathbf{r}_0|^2} = - \frac{\mu_0}{4\pi} \int_{v_0} \mathbf{M}(\mathbf{r}_0) \cdot \frac{(\mathbf{r} - \mathbf{r}_0)}{|\mathbf{r} - \mathbf{r}_0|^2} dv_0 \quad (5.22)$$

Similarly, the last equation can also be stated as

$$V_B(\mathbf{r}) = \frac{\mu_0}{4\pi} \int_{v_0} \mathbf{M}(\mathbf{r}_0) \cdot \nabla \left(\frac{1}{|\mathbf{r} - \mathbf{r}_0|} \right) dv_0 \quad (5.23)$$

Poisson relation:

For an arbitrary body as mentioned above, there exists a relationship between different fields due to the fact that they are generated by “the same geometric shape”. In geophysical applications, this relationship can be applied to gravitational and magnetostatic fields. That is, if we assume that a body of finite volume has a uniform density (ρ) and magnetization (\mathbf{M}), then these terms can be taken outside of (5.18) and (5.23), and we obtain

$$U(\mathbf{r}) = G\rho \int_{v_0} \frac{1}{|\mathbf{r} - \mathbf{r}_0|} dv_0 \quad (5.24)$$

and

$$V_B(\mathbf{r}) = \frac{\mu_0 \mathbf{M}}{4\pi} \int_{v_0} \nabla \left(\frac{1}{|\mathbf{r} - \mathbf{r}_0|} \right) dv_0 \quad (5.25)$$

Note that the integrands are now only functions of the geometry. In (5.25), if the gradient operator is further replaced by the directional derivative of the magnetization using the geometric relation (5.13), then the magnetic potential can be written as

$$V_B(\mathbf{r}) = \frac{\mu_0 M}{4\pi} \int_{v_0} \frac{\partial}{\partial d} \left(\frac{1}{|\mathbf{r} - \mathbf{r}_0|} \right) dv_0 \quad (5.26)$$

Here, d represents the direction of the magnetization vector as defined before. Since the direction of magnetization is uniform throughout the volume, the directional derivative can be further taken outside of the integral in (5.26), i.e.

$$V_B(\mathbf{r}) = \frac{\mu_0 M}{4\pi} \frac{\partial}{\partial d} \int_{v_0} \left(\frac{1}{|\mathbf{r} - \mathbf{r}_0|} \right) dv_0 \quad (5.27)$$

Equating the integral terms of (5.24) with (5.27) results in

$$V_B(\mathbf{r}) = \frac{\mu_0}{4\pi G} \frac{M}{\rho} \frac{\partial}{\partial d} U(\mathbf{r}) \quad (5.28)$$

Furthermore, if the gradient operator acts on both sides, one also gets a relation for the force fields as

$$\mathbf{B}(\mathbf{r}) = -\frac{\mu_0}{4\pi G} \frac{M}{\rho} \frac{\partial}{\partial d} \mathbf{g}(\mathbf{r}) \quad (5.29)$$

where we used $\mathbf{B} = -\nabla V_B$ for the magnetic potential, similar to the definition of electric potential. This equation is known as the *Poisson relation* between gravitational and magnetic fields due to a body in space. Equation (5.29) states that if the density and magnetic properties of the subsurface body are known, then it is possible to generate one field from the other. Assuming a linear relationship between density and magnetic properties of rocks, Poisson relation can be practically applied in geological problems (Baranov, 1957).

In theory, similar relationships can be obtained between the electrostatic field and the gravitational or magnetostatic fields; however this is practically not useful for the Earth systems applications as the finite conductivity of the rocks does not allow existence of electrostatic sources inside the Earth.

5.c. Green's functions for static fields

The volumetric integrals above can be derived from our previous formulation of the Green's function associated with the Laplacian operator. For the gravitational field, Poisson's equation (5.4) has the form of equation (4.16) with $f(\mathbf{r}) = -4\pi G\rho(\mathbf{r})$. Hence, the gravitational field can be written according to equation (4.17) as

$$U(\mathbf{r}) = G \int_{v_0} \frac{\rho(\mathbf{r}_0)}{|\mathbf{r} - \mathbf{r}_0|} dv_0, \quad (5.30)$$

where Green's function, by equation (4.19), is

$$G_U(\mathbf{r}, \mathbf{r}_0) = G \frac{1}{|\mathbf{r} - \mathbf{r}_0|}. \quad (5.31)$$

Similarly, for a static electric source, equation (5.8) implies $f(\mathbf{r}) = -Q(\mathbf{r})/\varepsilon_0$ in (4.16), and (4.17) yields

$$V_E(\mathbf{r}) = \frac{1}{4\pi\epsilon_0} \int_{v_0} \frac{Q(\mathbf{r}_0)}{|\mathbf{r} - \mathbf{r}_0|} dv_0, \quad (5.32)$$

for the electrostatic potential, with Green's function

$$G_E(\mathbf{r}, \mathbf{r}_0) = \frac{1}{4\pi\epsilon_0} \frac{1}{|\mathbf{r} - \mathbf{r}_0|} \quad (5.33)$$

Finally, for a magnetic field source, (5.23) can be written as

$$V_B(\mathbf{r}) = \int_{v_0} \mathbf{M}(\mathbf{r}_0) \cdot \left[\frac{\mu_0}{4\pi} \nabla \left(\frac{1}{|\mathbf{r} - \mathbf{r}_0|} \right) \right] dv_0 = \int_{v_0} M \left[\frac{\mu_0}{4\pi} \nabla_d \left(\frac{1}{|\mathbf{r} - \mathbf{r}_0|} \right) \right] dv_0 \quad (5.34)$$

Then, Green's function for magnetic potential becomes

$$G_B(\mathbf{r}, \mathbf{r}_0) = \frac{\mu_0}{4\pi} \nabla_d \left(\frac{1}{|\mathbf{r} - \mathbf{r}_0|} \right) \quad (5.35)$$

The subscript d represents the directional derivative in the direction of magnetization.

5.d. Maxwell equations in free space

As mentioned before, both electric and magnetic fields are created by electric sources. Although the electric field can be formed by stationary electric sources, a magnetic field can only arise by moving electric sources (and an accompanying transient electric field), which cause generation of electromagnetic fields. The behavior of electromagnetic fields is described by four fundamental equations called *Maxwell's equations* (discussed below). Two of Maxwell's laws are related to the gradients of the force fields, which are already derived above. That is, if Laplace's equation for electric and magnetic potentials is stated for the vector fields \mathbf{E} and \mathbf{H} ¹, then one derives the Gauss law for electric and magnetic fields in free space

$$\nabla \cdot \mathbf{H} = 0 \quad (5.36)$$

$$\nabla \cdot \mathbf{E} = 0 \quad (5.37)$$

The other two Maxwell equations (in a source-free medium) describe the curls of the \mathbf{E} and \mathbf{H} fields as

$$\nabla \times \mathbf{H} = \epsilon_0 \frac{\partial \mathbf{E}}{\partial t} \quad (5.38)$$

¹ The magnetic fields strength (\mathbf{H}) is related to the magnetic field induction (\mathbf{B}) by $\mathbf{B} = \mu_0 \mathbf{H}$. In this section, we use \mathbf{H} instead of \mathbf{B} for describing the magnetic field since \mathbf{E} and \mathbf{H} are physically analogous fields, which will be more apparent in the following sections.

$$\nabla \times \mathbf{E} = -\mu_0 \frac{\partial \mathbf{H}}{\partial t} \quad (5.39)$$

Equations (5.36-5.39) completely describe the behavior of electromagnetic fields in free space. As seen in (5.38) and (5.39), electromagnetic fields are not curl-free, and therefore not conservative.

Using the four equations above, one can get equations for \mathbf{E} alone. If we take the curl of (5.39) on both sides and substitute into (5.38) for the curl of \mathbf{H} , we obtain

$$\nabla \times (\nabla \times \mathbf{E}) = -\mu_0 \frac{\partial}{\partial t} (\nabla \times \mathbf{H}) = -\epsilon_0 \mu_0 \frac{\partial^2 \mathbf{E}}{\partial t^2} \quad (5.40)$$

Use the identity (4.3) along with (5.37) we obtain

$$\nabla^2 \mathbf{E} - \mu_0 \epsilon_0 \frac{\partial^2 \mathbf{E}}{\partial t^2} = 0 \quad (5.41)$$

Similarly, an equation for the \mathbf{H} field can be obtained by taking the curl of (5.38), and substituting into (5.39):

$$\nabla^2 \mathbf{H} - \mu_0 \epsilon_0 \frac{\partial^2 \mathbf{H}}{\partial t^2} = 0 \quad (5.42)$$

The solutions for the \mathbf{E} and \mathbf{H} fields in (5.41) and (5.42) in free space have the form of the wave equation. In the wave equation, the speed of the wave is described as inverse square-root of the coefficient of the time-derivative; then, both fields have the same speed of $c = 1/\sqrt{\epsilon_0 \mu_0} = 2.998 \times 10^8$ m/s, the speed of light.

The differential equations (5.41-5.42) can be solved separately for both fields using the method of separation of variables, which yields the plane wave solutions (Menke and Abbott, 1990) as

$$\mathbf{E} = \mathbf{e} \cdot e^{i\mathbf{k} \cdot \mathbf{r} - i\omega t} \quad \text{and} \quad \mathbf{H} = \mathbf{b} \cdot e^{i\mathbf{k} \cdot \mathbf{r} - i\omega t} \quad (5.43)$$

Here \mathbf{e} and \mathbf{b} are the (unit length) polarization vectors whereas \mathbf{k} is the propagation vector of the field. The propagation and polarization vectors are related as

$$\mathbf{k} \times \mathbf{e} = \mathbf{b} \quad , \quad \text{and} \quad \mathbf{k} \times \mathbf{b} = \mathbf{e} \quad (5.44)$$

Therefore, we conclude that solution of Maxwell equations in source-free medium gives a solution where both fields propagate synchronously in direction of \mathbf{k} (direction of propagation), and \mathbf{E} and \mathbf{H} fields are in a direction perpendicular to both to the direction of propagation (transverse waves), and to each other.

6. Fields in sourced media:

As mentioned previously, interaction of fields in a medium with sources can cause secondary phenomena. Due to the very fundamental property of electric and magnetic sources being dipolar, \mathbf{E} and \mathbf{H} fields polarize the medium with electric or magnetic sources as they interact. This results in the creation of secondary fields in the medium. Since these secondary effects are material dependant, they form the basis of the methods used in geophysical prospecting.

6.a. Electric and magnetic polarization in source media

Electrical polarization:

The effect of polarization is easier to see in the case of an electric field (Figure 6.1 a-b). If the medium is disturbed by an external electric field, the charges inside the atoms move (displace) with respect to each other. This causes a secondary electric dipolar field around each atom (Figure 6.1b). As a result, the total electric field changes due to the polarization of the atoms. If the total polarization field is represented by the vector \mathbf{P} , the resulting field can be stated as

$$\mathbf{D} = \epsilon_0 \mathbf{E} + \mathbf{P} \quad (6.1)$$

The new field \mathbf{D} is called the *electric displacement*. The displacement \mathbf{D} includes both the effect of the external field and the field due to the polarization of atoms inside the matter. The amount of polarization is material dependent and (by experiment) is generally a linear function of the external electric field:

$$\mathbf{P} = \chi_e \mathbf{E} \quad (6.2)$$

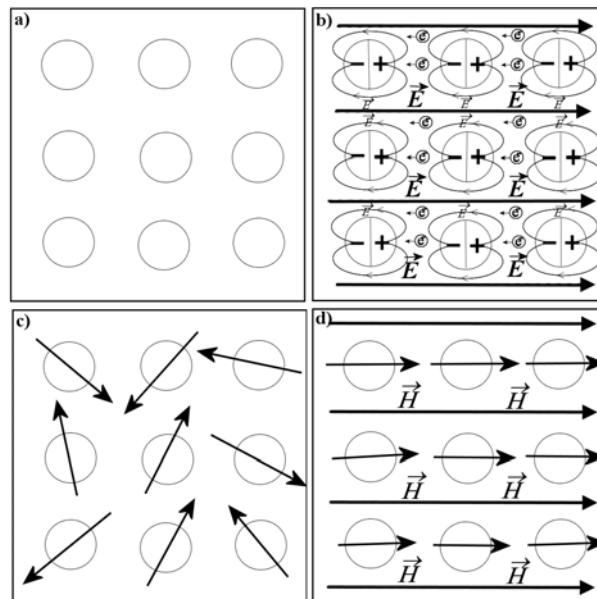


Figure 6.1 Polarization (a-b) and magnetization (c-d) phenomena in sourced media. In the left panels no external field is applied in the medium where sources exist. In the right panels, sources reconfigure according to the external field.

where χ_e represents the electric susceptibility tensor. It is a scalar quantity if the matter is isotropic. Then the displacement and electric field are related by

$$\mathbf{D} = \varepsilon_0 \mathbf{E} + \chi_e \mathbf{E} = (\varepsilon_0 + \chi_e) \mathbf{E} = \varepsilon \mathbf{E} \quad (6.3)$$

In the last equation ε is called the electric permittivity; and we can define a dimensionless quantity

$$\eta = \frac{\varepsilon}{\varepsilon_0} \quad (6.4)$$

which is called *the dielectric constant* of the material. Contrasts in dielectric properties of rocks set the basic working principle of the GPR method (discussed later in detail).

Magnetization:

Just as the electric field perturbs the charge distribution in a material, an external magnetic field also leads to the creation of secondary currents which leads to the creation of a secondary magnetic field inside the material (Figure 6.1d). The total magnetic field can then analogously be written as

$$\mathbf{B} = \mu_0 (\mathbf{H} + \mathbf{M}) \quad (6.5)$$

where \mathbf{M} represents the magnetization of the medium due to the external field and has the same unit as the magnetic field strength. Similar to the polarization in the case of electric fields, magnetization is also observed to be linearly dependent by a tensor relation to \mathbf{H} :

$$\mathbf{M} = \chi_m \mathbf{H} \quad (6.6)$$

The magnetic susceptibility χ_m is a dimensionless quantity in the SI system. In the case of an isotropic material, it is a scalar, which implies that \mathbf{M} is in the same or opposite direction as the ambient field \mathbf{H} . Then, (6.5) can also be stated as

$$\mathbf{B} = \mu_0 (\mathbf{H} + \chi_m \mathbf{H}) = \mu_0 (1 + \chi_m) \mathbf{H} = \mu \mathbf{H} \quad (6.7)$$

The coefficient μ is defined as the *magnetic permeability* of the medium. The ratio

$$\mu_r = \frac{\mu}{\mu_0} \quad (6.8)$$

is called the *relative permeability* of the material. In the magnetostatic method, any of the material dependant parameters mentioned above (i.e., susceptibility, permeability, or relative permeability) can be used as proxy, although susceptibility variations of Earth materials are more commonly used.

In conclusion, we observe that the polarization behavior of mediums under electric or magnetic fields show very similar characteristics. Equations (6.3) and (6.7) are called constitutive relations in electromagnetism. These relations are useful in hiding the secondary effects of polarization and magnetization in a medium with sources. We finally point out that both polarization and magnetization effects are due to the existence of electric charges in the environment, yet they can be treated completely independently. Both concepts have applications in the study of exploration geophysics.

6.b. Maxwell equations in sourced media

On microscopic scales, Maxwell's equations universally explain the electric field and magnetic induction phenomena by the following four equations:

Gauss law:	$\nabla \cdot \mathbf{E} = \frac{Q}{\epsilon_0}$	(6.9)
Gauss law for magnetism:	$\nabla \cdot \mathbf{H} = 0$	(6.10)
Faraday's law of induction	$\nabla \times \mathbf{E} = -\mu_0 \frac{\partial \mathbf{H}}{\partial t}$	(6.11)
Ampere's Law:	$\nabla \times \mathbf{H} = \mathbf{j} + \epsilon_0 \frac{\partial \mathbf{E}}{\partial t}$	(6.12)

where \mathbf{j} represents the electric current density. However, in sourced media, polarization and magnetization effects mentioned above can make the application of *the microscopic Maxwell equations* complicated. Then, on scales larger than atomic dimensions, one can use spaced-averaged properties of the fields, which hides the polarization and magnetization of the fields by the use of constitutive equations (6.3 and 6.7). Using the constitutive equations, *the macroscopic Maxwell equations* can be redefined as

$$\nabla \times \mathbf{H} = \mathbf{j} + \frac{\partial \mathbf{D}}{\partial t} \quad (6.13)$$

$$\nabla \times \mathbf{E} = -\frac{\partial \mathbf{B}}{\partial t} \quad (6.14)$$

$$\nabla \cdot \mathbf{B} = 0 \quad (6.15)$$

$$\nabla \cdot \mathbf{D} = Q \quad (6.16)$$

with the constitutive relations

$$\mathbf{D} = \epsilon \mathbf{E} \quad (6.17)$$

$$\mathbf{B} = \mu \mathbf{H} \quad (6.18)$$

$$\mathbf{j} = \sigma \mathbf{E} \quad (6.19)$$

The last equation (6.19) is an experimentally determined formula which relates the electric conduction in the medium with the external electric field, and is called *Ohm's law*. The coefficient σ is called the electric conductivity (inverse of resistivity) of the medium, and is another proxy used in geophysical prospecting. Once again, macroscopic Maxwell equations (6.14-16) along with the constitutive relations (6.17-19) hides the polarization effects that occur at atomic or molecular scales, and completely define behavior of electric/magnetic fields in any type of environment in an elegant way (as long as the working dimension of the problem is larger than atomic/molecular scales).

In geophysical applications, slowly varying fields are usually used in order to obtain enough penetration of electromagnetic waves into the subsurface. In this case, the electric properties of the minerals ε , μ and σ are nearly independent of the applied fields, allowing the \mathbf{E} and \mathbf{H} fields to be stated explicitly in the macroscopic Maxwell equations (6.13-16) using the constitutive relations (6.17-19). Furthermore, due to the finite amount of conductivity inside the rocks, no charge accumulation occurs inside medium, which means ($Q=0$) in (6.16). In this case, the most general forms of the Maxwell equations used in geophysical applications are

$$\nabla \times \mathbf{H} = \sigma \mathbf{E} + \varepsilon \frac{\partial \mathbf{E}}{\partial t} \quad (6.20)$$

$$\nabla \times \mathbf{E} = -\mu \frac{\partial \mathbf{H}}{\partial t} \quad (6.21)$$

$$\nabla \cdot \mathbf{H} = 0 \quad (6.22)$$

$$\nabla \cdot \mathbf{E} = 0 \quad (6.23)$$

For many practical applications, it is desirable to state the electric and magnetic field equations separately. This can be done by following a similar substitution procedure performed for the derivation of the electromagnetic wave equations in free space above (Section 5.d). As a result of this, one obtains the *telegrapher's equations*:

$$\nabla^2 \mathbf{E} - \mu \varepsilon \frac{\partial^2 \mathbf{E}}{\partial t^2} - \mu \sigma \frac{\partial \mathbf{E}}{\partial t} = 0 \quad (6.24)$$

$$\nabla^2 \mathbf{H} - \mu \varepsilon \frac{\partial^2 \mathbf{H}}{\partial t^2} - \mu \sigma \frac{\partial \mathbf{H}}{\partial t} = 0 \quad (6.25)$$

which constitute the most general form of the Maxwell equations used in a homogenous medium. Note that (6.24) and (6.25) are neither wave equations nor the diffusion equations, but a combination of both. Depending on the applications, either the second (radiation) or the third (diffusion) terms can be neglected leaving us with either the wave or diffusion equations (see below).

Behavior of electromagnetic waves can also be understood using the concept of wave number k (see the vector definition, $k=|\mathbf{k}|$, in Section 5.d). Electromagnetic waves can be approximated as plane waves with a time dependence factor of $e^{-i\omega t}$ as long as they are far from

their sources (Zhdanov and Keller, 1994). If the time derivatives act on these time dependant parts, equations (6.24) and (6.25) take the form of

$$(\nabla^2 + k^2)\mathbf{E} = 0 \quad (6.26)$$

$$(\nabla^2 + k^2)\mathbf{H} = 0 \quad (6.27)$$

where the wave number k is defined as

$$k^2 = \omega^2 \mu \varepsilon + i \omega \mu \sigma \quad (6.28)$$

Equations (6.26) and (6.27) are known as *Helmholtz equations*. The wave number defined in (6.28) bears a lot of insight toward understanding the behavior of the fields. That is, the first term represents the effect of displacement current whereas the second term represents the conduction currents in the propagation of electromagnetic waves. Depending on the frequency of the field, the first or the second term dominates and allows certain approximations to be made in the solutions. At high frequencies (e.g., range of GPR method), the dielectric properties of the medium dominantly control the propagation of the field without significant loss of energy (in general, energy loss is mainly controlled by electric conduction whereas energy loss associated with electric displacement is negligibly small). At this frequency range, the finite conductivity of the medium plays role only for the dissipation of the wave amplitude, whereas its role in the behavior of the field is negligibly small. On the other hand, at low frequencies (e.g., range of EM induction method), propagation of the fields is controlled by conductive properties of the medium, and the effects of displacement (i.e., the second term in (6.28)) are now negligibly small. Also in this range, the energy loss mechanism is by conduction.

The boundary between the diffusive or wave behaviors can be drawn using the parameter called *the loss factor*, which is defined as the magnitude of the ratio of the second term to the first in (6.28):

$$\delta = \frac{\sigma}{\omega \varepsilon} \quad (6.29)$$

The loss factor is often expressed by *the loss tangent*:

$$\tan \xi = \frac{\sigma}{\omega \varepsilon} \quad (6.30)$$

For the loss tangent greater than unity the electromagnetic field is said to be in the *quasi-stationary form*, whereas if it is less than unity, the fields are in the *radiation form*. This division greatly simplifies the analyses of the electromagnetic waves in different circumstances.

Quasi-stationary fields:

In most of the applications of electrical prospecting, low frequency waves (=quasi-stationary fields) are used in order to get deep penetration. In this case, the second time derivative of the fields in the telegrapher's equations (5.26-5.27) are very small and can conveniently be ignored. Then the equations become

$$\nabla^2 \mathbf{E} - \mu\sigma \frac{\partial \mathbf{E}}{\partial t} = 0 \quad (6.31)$$

$$\nabla^2 \mathbf{H} - \mu\sigma \frac{\partial \mathbf{H}}{\partial t} = 0 \quad (6.32)$$

These equations are in the form of a diffusion equation within a conducting medium (they diffuse into the medium as in a decaying chemical species diffusing in a tank) with the diffusion constant of $D=1/\mu\sigma$.

For quasi-stationary fields, the wave number takes a complex form:

$$k = \sqrt{i\omega\mu\sigma} = (1+i)(\omega\mu\sigma/2)^{1/2} \quad (6.33)$$

The magnitude of k can be used to define the wavelength (λ) of the EM field as

$$k = 2\pi/\lambda = (\omega\mu\sigma/2)^{1/2} \quad (6.34)$$

In practice, variations in the magnetic properties of Earth's materials are not very different from that of air (see Table 8.1) so one can substitute $\mu \approx \mu_0 = 4\pi \times 10^{-7}$ and the wavelength for the quasi-stationary field becomes

$$\lambda = (10^7 RT)^{1/2} = 503.3\sqrt{RT} \quad (6.35)$$

Here we made the substitutions $R=1/\sigma$ where R stands for electric resistivity, and $\omega = 2\pi T^{-1}$ as the quasi-stationary fields are generally described by their periods (T) rather than frequencies. It should be pointed out that although the quasi-stationary fields are also represented by characteristic wavelengths like radiation fields, they are not actually "waves" in the quasi-stationary approximation, and they interact with the medium following the diffusion equation rather than the wave equation.

Radiation fields:

At high frequencies, the conductive behavior of the medium is less responsive to propagation behavior and the third terms in telegrapher's equations can be ignored. In this case, we get the wave equations:

$$\nabla^2 \mathbf{E} - \mu\epsilon \frac{\partial^2 \mathbf{E}}{\partial t^2} = 0 \quad (6.36)$$

$$\nabla^2 \mathbf{H} - \mu\epsilon \frac{\partial^2 \mathbf{H}}{\partial t^2} = 0 \quad (6.37)$$

which have identical solutions for the electromagnetic fields in free space (5.41-42) with the exception that the permeability (μ) and permittivity (ϵ) are specific to the medium. As a result of

this, the wave speed inside the medium becomes $c' = 1/\sqrt{\epsilon\mu}$, which is slower than the speed of light. Equations (6.36-37) carry exactly the same characteristics of the fields in free space, and can also be represented by the plane wave solution (i.e. 5.43 and 5.44).

Stationary Fields in an insulating medium

For the stationary external \mathbf{E} and \mathbf{H} fields, if no conduction is allowed in the medium ($\sigma=0$) but there is a non-zero stationary charge density distribution, then the Maxwell equations take the form of two sets of independent equations for the \mathbf{E} and \mathbf{B} fields; one forms the *electrostatic field* and the other forms the *magnetostatic field*.

$$\nabla \times \mathbf{H} = 0 \tag{6.38}$$

$$\nabla \cdot \mathbf{B} = 0 \tag{6.39}$$

$$\nabla \times \mathbf{E} = 0 \tag{6.40}$$

$$\nabla \cdot \mathbf{D} = Q \tag{6.41}$$

This condition is identical to the treatment of \mathbf{E} and \mathbf{B} fields due to static point sources that was discussed previously. The addition is that the constitutive equations, i.e.,

$$\mathbf{D} = \epsilon\mathbf{E} \tag{6.42}$$

$$\mathbf{B} = \mu\mathbf{H} \tag{6.43}$$

In this case, both electrostatic and magnetostatic fields are curl-free and can be written as a gradient of scalar potentials

$$\mathbf{E} = -\nabla V_E \qquad \mathbf{B} = -\nabla V_B \tag{6.44}$$

We point out again that electrostatic theory does not normally find applications in the study of Earth's interior since no charge accumulation occurs inside the Earth as a result of the finite conductivity of rocks (i.e. equation (6.41) is homogeneous).

Stationary fields in a conducting medium:

In a conducting medium with stationary electric and magnetic fields, the Maxwell equations have the form of

$$\nabla \times \mathbf{H} = \mathbf{j} \tag{6.45}$$

$$\nabla \cdot \mathbf{H} = 0 \tag{6.46}$$

$$\nabla \times \mathbf{E} = 0 \tag{6.47}$$

$$\nabla \cdot \mathbf{E} = 0 \tag{6.48}$$

with the constitutive equation

$$\mathbf{j} = \sigma \mathbf{E} \quad (6.49)$$

These forms of Maxwell's equations describe the behavior of currents inside a conductive medium. Here, the applied electric field produces a current flow (galvanic current) inside the medium which is accompanied by a static magnetic field as revealed by (6.45). As mentioned above, equation (6.48) is homogenous because of the fact that no charge accumulation occurs in a conductive medium. This also implies that the current flow is divergence free, i.e.,

$$\nabla \cdot \mathbf{j} = 0 \quad (6.50)$$

At this point, one can observe a complete mathematical analogy between the equations of the electrostatic field (6.40, 6.41 and 6.42; assuming no electric charge), the equations of a magnetostatic field (6.38, 6.39 and 6.43), and the equations of electric conduction (6.47, 6.50, and 6.49), respectively. This analogy allows us to use the solution of one field for the solution of the other; once the correct conversions of parameters are made. The parameter conversions are listed as follows:

Table 6.1 Analogy between parameters of electrostatic, magnetostatic and electric conduction

Electrostatic	Magnetostatic	Electric conduction
\mathbf{D}	\mathbf{H}	\mathbf{j}
ϵ	$1/\mu$	σ
q (total charge)	-0-	I (total current)

We note that although \mathbf{D} and \mathbf{H} are not the physically corresponding parameters in electromagnetism (i.e., \mathbf{D} involves polarization of the medium but \mathbf{H} is the secular magnetic field), they appear to be analogous parameters in the mathematical formulations.

Table 6.1 is a very helpful tool to convert equations from one field to another only by changing certain parameters. One application of this analogy is that one can write Green's function for electric conduction easily using the derivations of Green's function for the electrostatic field (5.33). Then, using the conversion table (Table 6.1), one can write

$$G_I(\mathbf{r}, \mathbf{r}_0) = \frac{1}{4\pi\sigma} \frac{1}{|\mathbf{r} - \mathbf{r}_0|} \quad (6.51)$$

for Green's function for electric conduction in a conductive medium.

6.c. Seismic Fields

Although they are physically completely different, the formulations of the seismic waves are analogous to those of the electromagnetic fields in an insulating medium (i.e. 6.36 and 6.37). Below is a rather summarized theory of seismic wave theory, which intends to show parallelisms with the previously mentioned fields.

The behavior of seismic waves can be represented by *Hooke's law*, which relates the stress (σ) to the strain (ε) on a spring by the following formula

$$\sigma = E\varepsilon \quad (6.52)$$

The spring constant (E : Young modulus) is a constitutive property depending on the elastic properties of the medium.

We start by stating Newton's law on a unit volume v with a surface area S . The displacement (\mathbf{u}), related to body forces (\mathbf{f}) and tractions due to neighboring bodies (\mathbf{t}) can be represented by the Newton's second law:

$$\sum F_i = \int_v f_i dv + \int_S t_i dS = \int_v \rho \frac{\partial u_i^2}{\partial t^2} dv = ma_i \quad (6.53)$$

Here, ρ , m , and a are density, mass, and acceleration of the unit body, respectively. The index i represents the component of the force along a particular direction. If the divergence theorem (4.5) is applied in the surface integral in (6.53), one obtains

$$\int_v \rho \frac{\partial u_i^2}{\partial t^2} dv = \int_v \left(f_i + \frac{\partial \sigma_{ij}}{\partial x_j} \right) dv \quad (6.54)$$

and

$$\rho \frac{\partial u_i^2}{\partial t^2} = f_i + \frac{\partial \sigma_{ij}}{\partial x_j} \quad (6.55)$$

For most cases in seismic fields the body forces (f_i) can be ignored. In the last equation the stress (σ) term can be written in terms of the displacement; however, a simple relationship between stress and displacement as shown in (6.52) does not exist in 2- or 3- dimensions. The *generalized Hooke's law* includes both dilatational and rotational displacement of the unit body which is linked by a rank-4 tensor, and in a homogenous, isotropic medium, it takes the form:

$$\sigma_{i,j} = c_{i,j,k,l} \varepsilon_{k,l} = (\lambda + \mu) \frac{\partial u_k}{\partial x_k} + \mu \frac{\partial u_i}{\partial x_i} \quad (6.56)$$

Here, the parameters λ and μ are related to the elastic properties of the medium. Then, the equation of motion (6.55) becomes

$$\rho \frac{\partial u_i^2}{\partial t^2} = (\lambda + \mu) \frac{\partial}{\partial x_i} \frac{\partial u_k}{\partial x_k} + \mu \nabla^2 u_i \quad (6.57)$$

and, in vector form

$$\rho \frac{\partial \mathbf{u}^2}{\partial t^2} = (\lambda + \mu) \nabla(\nabla \cdot \mathbf{u}) + \mu \nabla^2 \mathbf{u} \quad (6.58)$$

Using the identity (4.3), the last equation can also be written as

$$\rho \frac{\partial \mathbf{u}^2}{\partial t^2} = (\lambda + \mu) \nabla(\nabla \cdot \mathbf{u}) + \mu(\nabla \times \nabla \times \mathbf{u}) \quad (6.59)$$

On the right hand side of the last equation, the first term represents the dilatational behavior (*P*-waves) whereas the second term represents the rotational behavior (*S*-waves) of seismic waves. In practice, it is difficult to solve the wave equation (6.59) for displacement. Instead, one prefers to decompose the displacement (\mathbf{u}) into dilatational and rotational components. One way to do this is to use *Helmholtz theorem*, which states that any vector field can be stated as a combination of the gradient of a scalar potential and the curl of a vector potential i.e.

$$\mathbf{u} = \nabla \Phi + \nabla \times \Psi \quad (6.60)$$

If (6.60) is substituted in (6.59), one gets two separate equations for the scalar (Φ) and vector (Ψ) fields as

$$\nabla^2 \Phi = \frac{1}{\alpha^2} \frac{\partial^2 \Phi}{\partial t^2} \quad \text{where } \alpha = \sqrt{\frac{\lambda + 2\mu}{\rho}} \quad : \text{ speed of } P\text{-waves} \quad (6.61)$$

and

$$\nabla^2 \Psi = \frac{1}{\beta^2} \frac{\partial^2 \Psi}{\partial t^2} \quad \text{where } \beta = \sqrt{\frac{\mu}{\rho}} \quad : \text{ speed of } S\text{-waves} \quad (6.62)$$

By the definition of scalar and vector potentials (6.60), one can note that *P*-waves form a curl-free field whereas *S*-waves form a divergence-free field. In exploration seismology, the subsurface information is obtained using *P*-waves which are curl-free; and therefore form a conservative wave field.

7. Comparison of the formulation of the fields

The mathematical analysis performed here allows us to compare the different geophysical methods in terms of mathematical formulations. A broad analysis reveals that the formulations can be grouped into two main categories that are those for the stationary fields and the transient fields. Tables 7.1 and 7.2 show comparisons of the stationary and transient field equations respectively outlining the similarities and differences.

Apparently, analogies are more outstanding in the case of stationary fields. One of the most important common properties of all methods is that they are curl-free, and therefore possess the properties of conservative fields. Furthermore, their constitutive relations are also similar.

Table 7.1 Comparison of the mathematical relations for stationary fields

	Potential	Curl	Field equation	Constitut. Relation	Green's function
Gravitation	$\mathbf{g} = \nabla U$	$\nabla \times \mathbf{g} = 0$	$\nabla \cdot \mathbf{g} = 4\pi G\rho$	N/A	$\mathbf{G}_U(\mathbf{r}, \mathbf{r}_0) = G \frac{1}{ \mathbf{r} - \mathbf{r}_0 }$
Electrostatics	$\mathbf{E} = -\nabla V_E$	$\nabla \times \mathbf{E} = 0$	$\nabla \cdot \mathbf{E} = \frac{1}{\epsilon} Q$	$\mathbf{D} = \epsilon \mathbf{E}$	$G_E(\mathbf{r}, \mathbf{r}_0) = \frac{1}{4\pi\epsilon} \frac{1}{ \mathbf{r} - \mathbf{r}_0 }$
Magnetostatics	$\mathbf{B} = -\nabla V_B$	$\nabla \times \mathbf{B} = 0$	$\nabla \cdot \mathbf{B} = \mu_0 \nabla_d \mathbf{M}^*$	$\mathbf{H} = \frac{1}{\mu} \mathbf{B}$	$G_B(\mathbf{r}, \mathbf{r}_0) = \frac{\mu}{4\pi} \nabla_d \left(\frac{1}{ \mathbf{r} - \mathbf{r}_0 } \right)^*$
Electric conduction	$\mathbf{E} = -\nabla V_E$	$\nabla \times \mathbf{E} = 0$	$\nabla \cdot \mathbf{E} = \frac{1}{\sigma} J$	$\mathbf{j} = \sigma \mathbf{E}$	$G_I(\mathbf{r}, \mathbf{r}_0) = \frac{1}{4\pi\sigma} \frac{1}{ \mathbf{r} - \mathbf{r}_0 }$

* For the limiting case of a point dipole source.

The comparison of transient fields (Table 7.2) reveals no conservative-field correlation, with the exception that P-wave field for seismic waves which is conservative.

Table 7.2 Comparison of the mathematical formulation for transient fields

	Potential	Curl of the field	Field equation	Constitutive Eq.
E-M (quasi-static)	$\mathbf{H} = \nabla \times \mathbf{A}$ $\mathbf{E} = -\nabla U - \frac{\partial \mathbf{A}}{\partial t}$	$\nabla \times \mathbf{E} \neq 0$ $\nabla \times \mathbf{H} \neq 0$	$\nabla^2 \mathbf{E} = \sigma\mu \frac{\partial \mathbf{E}}{\partial t}$ $\nabla^2 \mathbf{H} = \sigma\mu \frac{\partial \mathbf{H}}{\partial t}$	$\mathbf{D} = \epsilon \mathbf{E}$ $\mathbf{B} = \mu \mathbf{H}$
E-M (radiation)	$\mathbf{H} = \nabla \times \mathbf{A}$ $\mathbf{E} = -\nabla U - \frac{\partial \mathbf{A}}{\partial t}$	$\nabla \times \mathbf{E} \neq 0$ $\nabla \times \mathbf{H} \neq 0$	$\nabla^2 \mathbf{E} = \epsilon\mu \frac{\partial^2 \mathbf{E}}{\partial t^2}$ $\nabla^2 \mathbf{H} = \epsilon\mu \frac{\partial^2 \mathbf{H}}{\partial t^2}$	$\mathbf{D} = \epsilon \mathbf{E}$ $\mathbf{B} = \mu \mathbf{H}$
Seismic	$\mathbf{u} = \nabla \Phi + \nabla \times \Psi$	$\nabla \times \mathbf{u} = 0$ (P-waves) $\nabla \times \mathbf{u} \neq 0$ (S-waves)	$\nabla^2 \Phi = \frac{1}{\alpha^2} \frac{\partial^2 \Phi}{\partial t^2}$ (P-waves) $\nabla^2 \Psi = \frac{1}{\beta^2} \frac{\partial^2 \Psi}{\partial t^2}$ (S-waves)	$\sigma = E\epsilon$ (Hooke's law)

An outstanding analogy does exist between the seismic and EM radiation fields, as they both follow the wave equation. As discussed in the next section, these two fields have strong commonalities from both theoretical and practical aspects.

Present Applications of the Geophysical Methods

8. Physical properties of earth materials

The degree of resolution from a particular geophysical method is contingent upon the variations of the subsurface properties being investigated. Table 8.1 is a simplified summary of the properties of common Earth materials. Variations of these properties along with the sensitivity of the measurement system determine the applicability of a geophysical method for a particular problem.

Table 8.1 Average physical properties of some materials encountered in geophysical applications (Data compiled from Clark, 1966; Telford et al., 1976; Parasnis, 1986; and Zhdanov and Keller, 1994)

	Material [#]	Density (g/cm ³)	Magnetic Susceptibility ($\mu / \mu_0 - 1$)	Log Resistivity (Ohm-m)	Dielectric constant (ϵ / ϵ_0)	Seismic velocity (km/sec)
Various	Air	0.001	0	15	1	0.3
	Water	1.0	-7×10^{-10}	0-2	80	1.4-1.5
	Ice	0.9	-7×10^{-10}	6	3-4	3.4
	Oil	0.6-0.9	2×10^{-5}	14	2	1.3
	Salt	2.2	-1×10^{-6}	15	6	4.5-5
Unconsolidated Sediments	Soil	1.5	$7 \times 10^{-4*}$	3	4	0.1-0.2
	Clastics	1.9	$5 \times 10^{-4*}$	3-4	4	1-2
	Sand	1.6	$5 \times 10^{-4*}$	4	4	3
Metal Ores	Oxides	3.8-9.1	3×10^{-3}	(-1)-2	10-25	5.8
	Sulfides	3.8-8.1	3×10^{-3}	(-6)-(-3)	8-31	5.5
Sedimentary rocks	Sandstone	2.2	$4 \times 10^{-4*}$	2-3	5	2-6
	Shale	2.1	$6 \times 10^{-4*}$	0-1	6-8	2.3
	Limestone	2.7	$3 \times 10^{-4*}$	2-3	8-9	3-6
Igneous Rocks	Granites	2.6	$2 \times 10^{-3*}$	4-6	5	5-6
	Basalt	3.0	$7 \times 10^{-2*}$	7	12	5-6
Metamorphics	All	2.6-2.7	$5 \times 10^{-3*}$	3-5	8-10	5.5-6

[#]For dry samples except water; * May show orders of magnitude variations.

For reference, $\mu_0 = 4\pi \times 10^{-7}$ ohm-s/m; $\epsilon_0 = 8.8 \times 10^{-12}$ F/m

As seen In Table 8.1, densities of Earth materials are similar to each other. The highest densities are associated with ore bodies, whereas the lowest densities are associated with air (a subsurface cavity).

Magnetic susceptibilities of rocks are generally very weak ($\sim 10^{-4}$) and show large variations (from virtually no susceptibility to values 3-4 orders of magnitude higher than shown in Table 8.1). The rock susceptibility is almost entirely determined by its concentration of mineral magnetite and also the grain sizes of these magnetite minerals (explained below). With highest magnetic contents with the smallest grains sizes, basalt has the highest magnetization among Earth materials. Lastly, as mentioned before, low magnetic susceptibilities of rocks ($\sim 10^{-4}$) allow the geophysicists who are modeling the Earth's electrical structure to take $\mu = \mu_0$ in most of the cases.

In terms of resistivities, we observe orders of magnitude differences among Earth materials. As metal-bearing deposits, oxides and sulfides have the lowest resistivities, but they are found only in localized areas. Among the commonly found constituents of the Earth subsurface, water and shale stand out with the lowest resistivities. Water conductivity can vary greatly depending on the dissolved salt content. Due to the high electrical conductivity of water, electric conduction in porous or fractured rocks is dominantly due to electrolytes inside the pores and fractures. As a result of this, the bulk resistivity of rocks is expressed as a function of its water saturation which is given by Archie's law (Zhdanov and Keller, 1994):

$$R_f = aR_w S^{-n} \phi^{-m} \quad (8.1)$$

Here, R_f and R_w represent the resistivities of the rock matrix and water, respectively, ϕ and S represent the porosity and saturation relative to volume; and a , m , and n are parameters for specific rock types; and their typical values are $a=0.5-2.5$, $m=1.3-2.5$, and $n \sim 2$. Note that (8.1) does not have a relationship to the resistivity of the rock matrix.

9. Static field methods

In total field methods one measures the gravitational or magnetic field on or above the surface of the Earth caused by subsurface sources. Since the measured field is a combination of many sources (including ones above the Earth), the measured field has to be deconvolved into components, which is a non-unique process. The degree of non-uniqueness can be decreased only by additional information about the sources.

The applicability of a particular total field method is contingent upon the sensitivity of the measurement system. Higher instrument accuracies bring a wider variety of applications of a particular method. Today, modern technologies allow very sensitive measurements of the gravitational and magnetic fields on or above the Earth. This also brings the need for accurate localization within a geodetic datum, which is possible with the GPS technology. These developments are very promising for future applications of the total field methods (Hansen, 2001).

9.a. Gravimetry

The purpose of gravimetry is to measure the gravitational acceleration and its variations on and above the Earth's surface. The knowledge of accurate and high-resolution gravitational field determinations find applications at all scales of geophysics, from understanding the core and mantle processes to monitoring water transport on the Earth fluid's envelope (NRC, 1997).

In geodetic terms, the gravity anomaly is related to the vertical gradient of the disturbing potential, T , defined as the difference between the potential of the geoid (W) and the potential of the reference ellipsoid (U),

$$T = W - U \quad (9.1)$$

The measurement of gravity is the measurement of the vertical gradient of W . Both W and U have centrifugal components due to the rotation of the Earth, but the disturbing potential is free from it, so T directly gives the gravitational field due to the disturbing source. Modern geodesy is

concerned with the accurate determination of the geoid as it is required for accurate determination of heights using GPS (Hofmann-Wellenhof and Moritz, 2005).

The value of gravitational acceleration in the SI system is $\sim 9.81 \text{ m/s}^2$ on the surface of the Earth. In most of the literature, one sees the units as Gal, which is equal to cm/s^2 . A convenient conversion can be made using $1 \text{ mGal} = 10 \text{ } \mu\text{m/s}^2$. To give an idea, moving 3 m away from the Earth results in decrease of $\sim 1 \text{ mGal}$ in the gravitational acceleration. Deviations of the geoid from the reference ellipsoid are around $\pm 30 \text{ mGal}$ with maximum values around $\pm 100 \text{ mGal}$ (NRC, 1997), and are called geoid undulations or geoid heights. As a local example, a static gravity anomaly due to a subsurface void of 2 m high and 1m wide at 5 m depth gives a peak of $13 \text{ } \mu\text{Gal}$, and can be discriminated using present gravity meters.

Gravity is measured in two general ways; one can measure directly the absolute value of the acceleration; or alternatively, one measures gravity differences with respect to a local reference point. Both are important in theoretical geodesy and gravimetry, and the latter is particularly appropriate for local exploration studies (Jekeli, 1987).

Absolute gravity measurements:

In absolute gravimetry, g_z is measured directly by the free fall of a test mass. The equation of motion can be stated as

$$a = g_z = \frac{d^2h}{dt^2} \tag{9.2}$$

where h and t denotes the height and time respectively. Obtaining accuracies in the order of μGal requires determination of distance and time with precision of $\pm 0.1 \text{ nm}$ and $\pm 0.1 \text{ ns}$, respectively. In order to achieve this level of accuracy, sophisticated physical tools have to be used. Distance is measured by laser interferometry and the time is measured by highly precise atomic clocks. These technological advances allow measurement of the absolute value of gravity to within a few μGals (Torge, 2001). The maximum accuracy in absolute gravity measurements is limited by factors such as temporal groundwater conditions, unmodeled systematic effects of the instruments, and variations in the effects of atmospheric loading.

Absolute gravity measurements are most useful as reference points for the relative gravity measurements (discussed below), which are key for the exact determination of geoid heights. Due to their high accuracies absolute gravity systems are used for monitoring the Earth's internal motions, including excitations of the Earth's core and free oscillations of the Earth after great earthquakes, as well as secular and periodic crustal deformations, among other geodynamical phenomena. Although absolute gravity measurements are often made at fixed locations, portable absolute gravimeters have been available for some time for greater applications to networks (Torge, 2001).

Relative gravity measurements:

In relative gravimetry, the gravitational acceleration is usually measured by means of spring-type gravimeters. The force on a spring with elastic constant of k depends linearly the on displacement, i.e.,

$$F = kx \sim mg \tag{9.3}$$

The advantage of relative gravity measurements is that one does not need to know values of either k or m in equation (9.3) as long as the gravimeter is calibrated by an absolute gravity datum. The commonly used method is a lever-arm, torsional spring balance where deviations of the test mass with respect to the equilibrium point are measured using optical and electronic techniques. Sensitivity of the spring system can be increased greatly by designing springs with very long effective period. This was achieved using the so-called zero-length spring implemented in an astatic (nearly unstable) configuration (LaCoste-Romberg gravimeter). These gravimeters can have sensitivities in the order of a few μGal although conventional instruments typically have precision of ~ 0.02 mGal (Chapin et al., 1999). The LaCoste-Romberg relative gravimeters are widely used from commercial to scientific studies because of their high sensitivity and portability. New designs include self leveling, which reduces the measurement time. The physical properties of the spring can change in time so the equipment has to be re-calibrated after certain time periods.

A special type of spring gravimeter measures the induced magnetic field due to disturbance of a test mass within magnetic field using a superconducting quantum interference device (SQUID). These instruments have sensitivities even below a μGal . The disadvantage of the superconducting gravimeters is that they are not portable. However, they are very useful in monitoring the temporal changes in gravity at a station due to various geodynamical processes.

Moving-base gravity measurements:

Moving-base (airborne/shipborne/helicopter) gravimetry is desirable for fast and efficient surveys over large areas and with high resolution. However, these systems have inherently less accuracy due to the non-gravitational acceleration effects, and the inaccuracy in leveling the platform. In moving-base systems, non-tractable high frequency kinematic effects are eliminated by averaging measurements along the track of the survey. So, moving-base measurements are also limited in spatial resolution.

The accuracy of shipborne surveys with spring lever gravimeters is about 1 mGal within a distance of ~ 1 km and slightly higher for helicopter surveys. Due to faster speeds of fixed-wing, airborne platforms, the spatial resolution is lower by a factor of about five, compared to the former ones (Torge, 2001). More modern systems measure all three components of the acceleration using an inertial navigation system (INS) and GPS (Jekeli, 1987; Jekeli, 1999; Jekeli and Kwon, 1999; Li and Jekeli, 2008). Accuracies of 3-7 mGal can be obtained over distances of 3-10 km.

Gravity gradiometry:

Measuring the gradient of the gravitational acceleration is a useful technique for a number of reasons. Since the gradient of g decays faster than g itself with distance, gradient signals from nearby sources are enhanced whereas signals of far sources are suppressed. This makes gravity gradiometry an ideal method for near-surface applications.

Another advantage of measuring the gradient is related to data acquisition on a moving platform. That is, the common mode acceleration of the vehicle is eliminated and the positioning accuracy requirements for the vehicle are also much less stringent. Modern gravity gradient measurements are obtained usually by differencing the outputs of two accelerometers. Different orientations of accelerometer pairs yield gradients in different directions. The unit of gravity gradient in SI is $1/\text{s}^2$; and 1 nano- $1/\text{s}^2$ is defined as 1 E (E standing for Eötvös).

The current accuracy of gravity gradiometers is in the order of 1 E in the static mode allowing for many near-surface applications. A disadvantage of static mode gradiometry surveys

is that they are prone to topographic disturbances requiring a rigorous topographic correction. However, this problem is mainly overcome in airborne and satellite applications. With the development of new technologies for reducing the noise levels and increasing the sensor accuracies; airborne gravity gradiometry has many potential applications in the near future (Jekeli, 2004).

Satellite gravity measurements:

Artificial satellites orbiting the Earth are in fact gravimeters by themselves. Due to their small masses with respect to the Earth's mass their orbital motion is dictated by the spatial variations in the Earth's gravitational field. Analogous to the free-fall absolute gravimeter, measuring the range of the satellites with respect to Earth-bound tracking stations yields information on the gravitational field at many of its spatial frequencies. The resulting model for the disturbing potential is directly proportional to a model of the geoid undulation. The resolution of the potential field (and geoid) determination using satellites is limited by the satellite altitude, which is often more than 1000 km. In order to obtain the Earth's geoid with high resolution and accuracy, dedicated gravity satellites have recently been launched (Rummel et al., 2002). These satellites fly at low orbital height (300-400 km) to increase the resolution of the determined geoid. For the most part they are dedicated satellites designed as orbiting gravity gradiometers, enabling in situ measurements, as opposed to the tracking method of field determination. Either two satellites are orbiting in tandem and accurately measure changes in their intersatellite distance (satellite-to-satellite tracking), or a single satellite carries accelerometer pairs (i.e., gradiometers) that measure gravitational gradients.

Gravitational field determination from satellite tracking is based on Newton's second law of motion modified for the existence of a field:

$$\ddot{\mathbf{x}} = \nabla V + \mathbf{a} \tag{9.4}$$

where the gravitational potential is expressed as a series of solid spherical harmonics (Kaula, 1966) in spherical coordinates

$$V(r, \theta, \lambda) = \sum_{n=0}^{n_{\max}} \sum_{m=0}^n \left(\frac{R}{r}\right)^{n+1} (C_{nm} \cos m\lambda + S_{nm} \sin m\lambda) P_{nm}(\theta) \tag{9.5}$$

where R is Earth's mean radius. The specific forces, \mathbf{a} , in equation (9.4) are determined using models of radiation pressure, atmospheric drag and other action-type accelerations imparted to the satellite. The observational data are the ranges to the satellite with respect to the known coordinates of tracking stations, and in essence yield the position vector of the satellite, \mathbf{x} . The coefficients of the potential field, $\{C_{nm}, S_{nm}\}$, also known as Stokes's coefficients, are solved by integrating the equations of motion, (9.4).

For dedicated gravity satellite missions, where in situ measurements are made as described above (see also Jekeli, 2007), the measurements are directly related to the potential, as given in equation (9.5), and a number of analytical methods exist to solve for Stokes's coefficients. In all cases, one must consider the temporal tidal effects of extra-terrestrial bodies, such as the moon and sun, and possibly other planets.

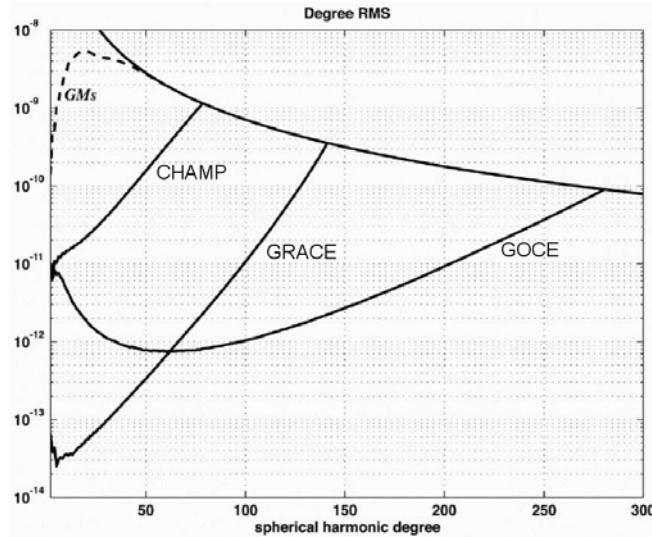


Figure 9.1 Relative accuracies of satellite gravity missions (modified from Rummel et al., 2002)

Three dedicated satellite gravity missions have been developed, and in part launched, in the last decade, each with a different design and capability, with their abbreviated names CHAMP, GRACE and GOCE (Rummel et al., 2002). Figure 9.1 summarizes roughly their relative, predicted measurement accuracies as a function of spherical harmonic degree, n . The superiority of dedicated mission over conventional satellites (GMs) is apparent in this figure. CHAMP (launched in 2000) uses the conventional method of satellite geodesy based on continuous GPS tracking, with the addition of an onboard accelerometer to improve the determination of the specific forces, a . GRACE (launched March 2002) is based on low-low satellite-to-satellite tracking using K-band ranging. The two satellites are about 200 km apart and the range velocity can be used to determine potential or gravitational differences (Jekeli, 2007). As seen in Figure 9.1, GRACE is superior to the other two missions below spherical harmonic degrees of 50 (400 km half-wavelength). The high accuracy of gravity field measurement of GRACE makes it possible to study the temporal variation of the field on global scales, such as the seasonal hydrological variations and co-seismic gravity changes following large earthquakes in the upper crust of the Earth (NRC, 1997). The third mission, GOCE (to be launched 2009), measures the various components of the gravitational gradient with three pairs of three-axis accelerometers. The working principle of GOCE is similar to GRACE in that both sense in situ gradients (differences) of gravitation, but GOCE yields higher resolution, although the lower frequencies of the field are not determined as well (Figure 9.1). With a lower altitude (250 km), GOCE is also able to take advantage of a higher signal-to-noise ratio.

Near-surface applications:

In near-surface applications, gravimetry demands far less than mGal accuracy, which, however, is readily achieved by current commercial gravimeters (Chapin, 1999), or gravity gradiometers. In such microgravity surveys, the nearby topographic features have to be taken into account and careful attention must be paid to any systematic errors, such as due to leveling errors that could produce signals comparable to the signal of the target.

For the detection of cavities, gravitational methods seem to be the best over other geophysical methods because of their high signal-to-noise ratio (Witten, 2006). The signal from a cylindrical cavity with a diameter of 4 m and at a depth of 4 m is ~ 0.06 mGal (Munk and Sheets, 1997), which can be detected using a conventional LaCoste-Romberg gravimeter. In

topographically flat terrain, unambiguous signals from caves were obtained using standard gravimeters (e.g., Rybakov et al., 2001; Styles et al., 2005; Witten, 2006; Mochales et al., 2008). Successful field studies using gravity combined with other methods such as GPR (Beres et al., 2001), and magnetic measurements and GPR (Mochales et al., 2008) have been reported. In cavity detection, the topographic effects should be carefully taken into account as nearby hills (<100 m in size) can give an impression of a cavity (Witten, 2006). Furthermore, downward undulations of the overburden and the water table variations can also produce signals similar to that of a cavity (McCann et al., 1987).

It has also been shown that gravity gradiometry can be a more powerful method in the detection of subsurface cavities, compared to direct gravimetry (Romaides et al., 2001). Especially, in areas with strong regional gravity trends, Romaides et al. (2001) reported that direct gravity signals was obscured; but gravity gradiometry measurements gave unambiguous signals.

In near surface problems, the lateral component of the residual field is comparable to the vertical component. As a result of this, it is conceivable that vector gravimetry would be more powerful over the vertical gravity measurements.

9.b. Magnetometry:

Although most of the Earth materials are non-magnetic in the absence of an external magnetic field, they show induced magnetization under the influence of the Earth's magnetic field. This phenomenon then can be used to get information of the subsurface structure. The ambient field of the Earth is in the range of 25000-60000 nT. Magnetic fields due to subsurface rocks are usually 1-100 nT for moderately magnetized bodies.

The magnetic field at some point is dependant on both the direction of the dipole source and the distance to the source (i.e., 5.15). As a result of the dipole source structure, unlike the gravitational field which is relatively smooth, the magnetic field above the surface can show rapid variations.

Magnetic properties of rocks

The magnetic behavior of materials is, in fact, more complex than was explained in Section 6. In comparison to electric sources, being free monopoles, magnetic sources in solids are dipoles, and they are frozen (i.e., non-conductive). The complexity of magnetic properties increases by interaction of individual dipole moments within a medium. As a result of this, magnetic property of a bulk material is not only dependant on individual dipole moments but also on the density and shape of dipole sources (mentioned subsequently). The net magnetic dipole moment of a material is the result of a combination of all these factors in a complex manner (Butler, 1992).

The basic sources of the dipole moment are the electrons in atoms each having a certain intrinsic dipole moment (Bohr magneton). An atomic or a molecular dipole moment forms as a result of an imbalance of electronic dipole moments. There are three common minerals in elemental forms that show magnetism even in the absence of an external magnetic field, which are Fe, Co and Ni; and they are the true *ferromagnetic* minerals (explained below). However, these substances are rarely found in nature and are not interesting in most of the discussions of magnetic behavior of Earth materials.

Dipole moments of molecules can be very different than atomic dipole moments as a result of exchanges of electrons between atoms. With the exception of the above mentioned natural magnets, minerals are not magnetic in the absence of an external magnetic field. According to their responses to an external magnetic field, minerals are divided into three groups (Figure 9.2).

In Figure 9.2 (graphs on the top line), the horizontal axis shows external magnetic field intensity (**H**) whereas the vertical axis shows the intensity of magnetization (**M**). According to (6.6) the slope of the curves gives the magnetic susceptibility (χ). In the first column of Figure 9.2 (9.2a), the mineral responds to an external field by a small amount of induced magnetic field in the direction opposite to the main field (i.e., $\chi < 0$). The induced field vanishes after the removal of the external field (no remnant magnetization). This behavior is said to be *diamagnetic* and is observed in all minerals which bear no magnetic atoms. The diamagnetism is not temperature dependent. In the second column (Figure 9.2b), minerals bear magnetic atoms in them but there is no interaction between the magnetic sources. They are called *paramagnetic* (Figure 9.2b). Paramagnetic minerals respond to an external magnetic field by an induced field in the same direction of the external field ($\chi > 0$) but the induced field vanishes after the removal of the external field. In the absence of an external magnetic field, all magnetic dipoles in a paramagnetic mineral are randomly oriented as a result of lack of interaction between them. The intensities of magnetization for diamagnetic and paramagnetic minerals are small and are not important in studying rock magnetism.

The third category is the most important one for rock magnetism. This group of minerals bears magnetic atoms like paramagnetic minerals, but these magnetic sources are also in interactions within the mineral (*ferromagnetism*², Figure 9.2c). In these minerals, application of an external field results in an induced field that is much stronger than that of diamagnetic and paramagnetic minerals. The most common types of ferromagnetic minerals are hematite and magnetite.

In ferromagnetic minerals, the relation between the external and induced field is represented by a *hysteresis curve* (Figure 9.2c, top). As seen in the figure, unlike diamagnetic and paramagnetic minerals, dependence of the induced field on the external field is not linear and very complex. For a ferromagnetic mineral, if an external magnetic field is gradually increased, the induced magnetic field also increases almost linearly (path 1 in Figure 9.2c). The induced magnetization reaches a point where it does not increase anymore for any increase in magnitude of the external field (saturation magnetization, **M_r** in Figure 9.2c). If the external field is decreased on the ferromagnetic material, the dipoles continue to interact with each other positively, and the mineral shows a finite magnetization even after total removal of the external field (path 2). *The remnant magnetization* is defined as the intensity of the magnetization with no external magnetic field (**M_r** in Figure 9.2c). Remnant magnetization is time dependent, and decays exponentially with time (Butler, 1992). Depending on the sizes and shapes of ferromagnetic grains in a rock, the relaxation time of remnant magnetization can be from seconds to millions of years (Butler, 1992). Materials with very short time of reminiscence are called *superparamagnetic* since they become non-magnetic after a short time of removal of the external magnetic field; so, they resemble paramagnetic minerals. This concept can be important in archeological studies if the host soil is disturbed by human activities and the time of magnetic relaxation of the soil is comparable to the age of the ruins (Witten, 2006). On the other hand, very long times of magnetic relaxation are important in paleo-tectonic studies (Butler, 1992).

² True definition of *ferromagnetism* is to have a non-zero intensity of magnetization even in absence of an external magnetic field (e.g., Fe, Co, Ni). Here the definition of ferromagnetism is made broader by including all the minerals with some kinds of interactions of dipoles within themselves. In fact, other names exist according to type of interactions of dipoles; they are either *antiferromagnetic* or *ferrimagnetic* (Clark, 1966). These are the ones commonly found in rocks in varying amounts and are responsible for bulk magnetic properties.

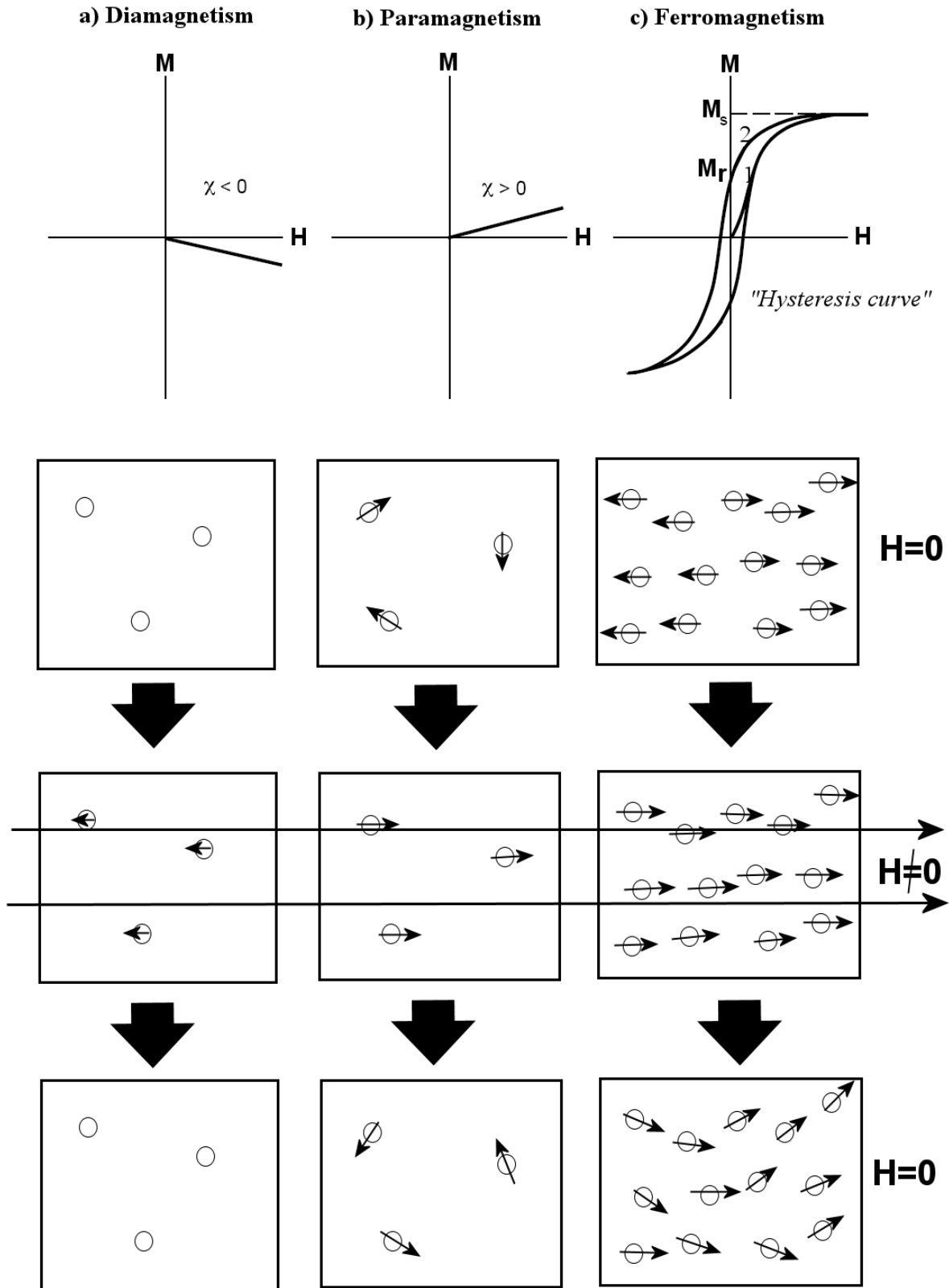


Figure 9.2 Types of magnetization in solids

For a magnetic mineral, both shape and size of grains are important and play crucial role in the bulk magnetic properties. In grains with large sizes and small aspect ratios, the magnetic sources tend to form separate domains (multi-domain (MD), Figure 9.3b). However, if the sizes of the grains become smaller, domain formation is no longer energetically favorable for the mineral so the entire grain becomes the domain itself (single-domain (SD), Figure 9.3a). The magnetization of SD grains is much larger than that of MD grains since in an MD grain magnetic vectors in opposite directions cancel each other giving a low net dipole moment (Figure 9.3b). For hematite and magnetite the critical grains sizes from MD to SD are $\sim 15 \mu\text{m}$ and $\sim 0.1 \mu\text{m}$, respectively, for cubic shapes. The larger SD grains are favorable in hematite because of the low internal magnetization of hematite mineral. For magnetite, the critical grain sizes are one order of magnitude smaller ($\sim 1 \mu\text{m}$) for elongated grains which are easily formed in fast cooling magmas. With high internal magnetizations, these SD grains show by far the strongest magnetization. A single magnetite mineral can host both SD and MD grains but the magnetic properties of the bulk mineral are almost totally controlled by SD grains.

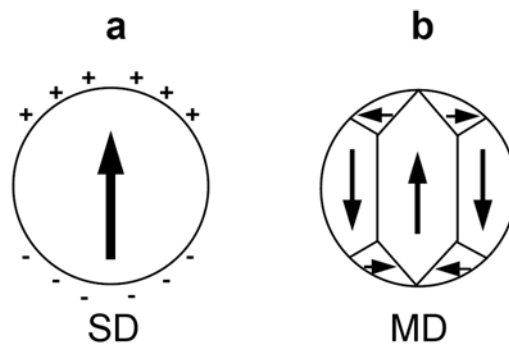


Figure 9.3 a) Single domain (SD) and b) Multi domain magnetisation of mineral grains (modified from Butler, 1992)

Rocks are formed by a combination of different minerals with varying types of magnetic properties. The bulk magnetic property of a rock is due to a combination of these individual components. However, due to peculiarities of magnetite mentioned above, its susceptibility is some 5 orders of magnitudes higher than all paramagnetic minerals and 2-3 orders of magnitude higher than hematite (Parasnis, 1986). As a *rock forming mineral* with a strong magnetization, magnetite was shown to be the biggest player in the determination of a bulk magnetic property of a rock (Clark, 1966; Butler, 1992). A less important player as a rock forming mineral is hematite which is a common mineral in sedimentary rocks.

A rock can exhibit induced (by ferromagnetic and paramagnetic grains) and remnant (by ferromagnetic grains only) magnetization simultaneously. For a rock, the ratio of remnant magnetization to induced magnetization is called *the Koenigsberger ratio*. In continental rocks (granites) this ratio may be from 0.01 to 3. Basalts in oceanic crust are perfect examples of elongated SD magnetite bearing rocks with remnant magnetization, and so the ratio is around 100.

Measurement methods:

Today's highly sensitive magnetic field measurement devices are categorized in two groups, which are vertical field (fluxgate and SQUID) and total field (proton precessing and alkali vapor) magnetometers.

Fluxgate method: In this method, a high susceptibility alloy rod (fluxgate) is used which responds parabolically to an applied magnetic field strength. The fluxgate is excited with a sinusoidally varying magnetic field using a coil around it. The resultant field within the fluxgate becomes

$$H = H_0 + p \sin \omega t \quad (9.6)$$

A secondary coil is used to measure the induction voltage due to the varying magnetic field inside the fluxgate. The amplitude of the voltage is both a function of the applied field and Earth's ambient field. The measured magnetic field is the component of the Earth's magnetic field along the direction of the fluxgate. This imposes a leveling restriction on the fluxgate method. The advantage is that one can measure the direction of the magnetic field vector, but on the down side, additional noise comes into the measurement due to leveling inaccuracies. The leveling requirement is less restrictive for measuring the vertical component of the induced magnetic field (ΔB_z) compared to the horizontal component (ΔB_h). The total field change (ΔB_t) is related to (ΔB_h) and (ΔB_z) anomalies through the following equation:

$$\Delta B_t = \Delta B_h \cos \alpha \cos I + \Delta B_z \sin I \quad (9.7)$$

where α and I represent the angles of declination and inclination, respectively. The vertical field of a magnetic anomaly (ΔB_z) is by far the best representative of a subsurface anomaly even close to equatorial regions where the vertical component of the magnetic field is low (Parasnis, 1986). As a result of this fact, in practical applications of the fluxgate method, one uses the vertical field variations only. The sensitivity of fluxgate instruments is in the order of 1 nT, but due to the leveling requirement, their practical sensitivities are in the order of ± 10 nT, and even less on moving platforms (Parasnis, 1986).

SQUID (Superconducting Quantum Interference Device): The working principle of a SQUID magnetometer is based on the simple fact that a time-varying magnetic field induces an electric current around a conducting coil. The superiority of a SQUID is that since the electric currents are formed in a superconducting medium at very low temperatures (using liquid nitrogen @77 K) the thermal noise is very low. In a virtually "noise-free" system, magnetic field changes of ~ 0.1 pT can be measured (Schmidt and Clark, 2006). In SQUIDs, only the magnetic field perpendicular to the coil is measured, so these measurements are directional as in fluxgate systems. SQUIDs are generally not used in regular magnetometry surveys due to practical problems, i.e. the cryogenic requirements. They have been recently suggested for use in airborne vector magnetic gradiometry systems (see below; Schmidt and Clark, 2006).

Proton precession method: It is well-known that protons (hydrogen atoms) have both an intrinsic magnetic moment and also an angular momentum. These isotopes can be concentrated in a liquid (e.g. water), which can be used to measure the strength of the magnetic field. That is, when a magnetic field is applied to the liquid, the protons start to precess around the direction of the applied magnetic field. Precession occurs due to the finite angular momentum of the protons. The frequency of the precession is a function of the applied magnetic field which is given by

$$\omega = \gamma B \quad (9.8)$$

where γ is a constant number (gyromagnetic ratio of the proton). Normally, the Earth's magnetic field is not strong enough to align the protons. In order to align the protons in one direction, a strong magnetic field is initially applied and protons are precessed in a certain direction. When the magnetic field is shut off, the protons still have their motion, but now they precess due to the Earth's magnetic field. Then, the precession frequency gives the magnitude of the magnetic field which is the Earth's magnetic field, itself. The advantage of the proton precession magnetometer is that the magnetic field is measured using the frequency of the electric signal, not any magnitudes, which results in accuracies of 0.1-1 nT. Since the frequency of the precession is only dependent on the magnitude of the field, no leveling is required. Due to this advantage of the proton precession method, it is often used for non-static applications such as airborne, shipborne and borehole measurements. The disadvantage of this method is that it only gives the magnitude of the total field.

Alkali vapor method: The general working principles of these magnetometers are the same as proton precession magnetometers. In these instruments, alkali atoms in ground states are excited to the states related to the external magnetic field using optical methods, and the decrease in the intensity of the light is measured. Sensitivities of these instruments are in the order of 0.01 nT. These are the preferred instruments over the regular proton precession magnetometers if higher sensitivities are desired.

Measuring the residual magnetic field

Earth materials have susceptibilities in the order of 10^{-3} (Table 8.1) which result in (volume normalized) field strengths of 25-60 nT close to their source locations. This number would be reduced by $1/r^3$ in a measurement location above the surface, and therefore the measured residual magnetic field becomes a small fraction of the total field. However, as mentioned above, accuracies of common magnetometers in geophysical applications are in the order of 0.1 nT, which makes the magnetic field measurements applicable almost without loss of generality.

Different magnetometers measure different components of the residual magnetic field depending on the type of magnetism. In the case of total field measurement (Figure 9.4a), a quantitative measurement can only be made for Earth's magnetic field that is much larger than the residual field. Nevertheless, this condition is met in most of the cases. On the other hand, a vertical field magnetometer exactly measures the vertical component of the residual (Figure 9.4b).

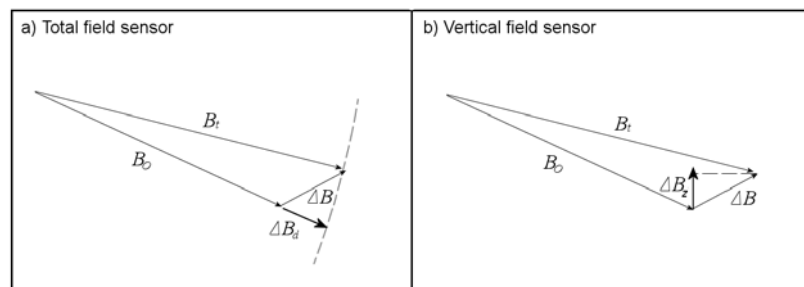


Figure 9.4 Measured component of residual field for a) total field sensors and b) vertical field sensor

Due to practical advantages of the proton precessing magnetometers, the total field is measured in most applications even though measuring the vertical variations (ΔB_z) is the best way for geologic interpretations. Magnetic field measurements are done with respect to a chosen reference point, and no absolute magnetic field is defined. In small area surveys (e.g. 1-10 km),

the Earth's field can be taken constant, but in large areas areal changes of the ambient field have to be considered. Vertical variations of the ambient field may also be important in some cases, which are in the order of 25 nT per km height (Parasnis, 1986).

Magnetic gradiometry:

The method of measuring the gradients of the magnetic field is also advantageous for the same reasons explained for gravity gradiometry (Schmidt and Clark, 2006). As an emerging field, magnetic gradiometry utilizes the superconducting quantum interference devices (SQUID), so it has the potential in the near future to delineate small susceptibility variations for near surface problems (Schmidt and Clark, 2006). Accuracies of 0.01 nT/m were claimed in magnetic gradiometry (Schmidt and Clark, 2006).

Near surface applications of magnetometry:

Near-surface applications of magnetometry are useful if the target has highly contrasting magnetic properties. Probably, the best example is in the detection of unexploded ordinances (UXO) (Butler et al., 2006). However, high instrument sensitivities make magnetometry also feasible for cases of low magnetizations. The magnetometric method was successfully applied for detection of underground cavities around the Dead Sea area (Rybakov et al., 2005), and showed perfect correlation with the earlier micro-gravity studies (Rybakov et al., 2001) in the same area. Recently, Mochales et al. (2008) used magnetometry (in combination with other methods) successfully for detecting and outlining shapes of sediment filled dolines. Another interesting application of near-surface magnetometry deals with the soil magnetic properties, which are unique from several aspects. First of all, their time constant for remnant magnetism is quite low making them superparamagnetic (explained above). Secondly, studies showed that soils generally have quite strong susceptibilities independent of their parent rocks, due partly to an ultrafine grained mineral called maghemite (Cook and Carts, 1962). One of the applications of magnetic studies in soils is in archeology where soil magnetic properties (direction of magnetization) are disturbed by recent (5,000-10,000 years) human activities. These buried disturbances can be detected using very sensitive magnetometers before any excavation activities begin (Witten, 2006).

9.c. MMR method:

One of the Maxwell equations for the stationary fields states that

$$\nabla \times \mathbf{H} = \mathbf{j}. \tag{9.9}$$

That is, when a current source is applied into the Earth, it is accompanied by a magnetic field at the surface. This magnetic field is formed by both current flowing above and below the surface. In DC resistivity methods, this magnetic field is ignored. However, the magnetic field formed by the galvanic currents (flowing inside the Earth) can also be used to obtain information of the subsurface structure. In the magnetometric resistivity (MMR) method, a rather useful equation that relates the induced magnetic field due to a current source was first formulated by Biot – Savart (before the emergence of Maxwell's equations) as

$$d\mathbf{B} = \frac{\mu}{4\pi} \frac{I \cdot d\mathbf{l} \times \mathbf{r}}{r^2}. \tag{9.10}$$

The last equation is known as *Biot-Savart law* and is essentially a different form of one of the Maxwell equations. Here $d\mathbf{l}$ represents the infinitesimal length of the current flowing in the medium and \mathbf{r} represents the distance to the measurement point. The Biot-Savart law can be manipulated in a useful form for subsurface applications so that the total magnetic field measured above the surface is written as a function of the electrical potential (V_E) and the electric conductivity (σ) of the medium. Following the derivation of Edwards et al. (1978) the total magnetic field can be written by the following integral:

$$\mathbf{B}(\mathbf{r}) = \frac{\mu}{4\pi} \int_{v'} \frac{\nabla V_E(\mathbf{r}') \times \nabla \sigma(\mathbf{r}')}{|\mathbf{r} - \mathbf{r}'|} dv' \quad (9.11)$$

The measured magnetic field here represents the MMR signal due only to currents passing through the subsurface. Equation (9.11) bears information related to certain advantages of the MMR method over other conventional electric methods, which is a direct result of the gradient of the electric conductivity ($\nabla \sigma$) in the integrand. First of all, in a homogeneous medium, the gradient of the conductivity of the medium is zero everywhere except at the surface where it is vertical, so an electrically uniform medium will have no MMR signal. The MMR signal will only occur if there is a discontinuity in the conductivity of the subsurface. A second advantage comes from the vector product in the integrand of (9.11) as no vertical MMR anomaly will occur in a horizontally stratified Earth, since the gradient of the conductivities will all be vertical in this case. This may be useful in all cases where the vertical resistivity variations of the Earth impose additional complications to the solution. Due to these peculiarities, it has been argued that the MMR method is advantageous over other electric methods for being able to detect structures below conducting overburdens, and also for anomalies within conductive hosts (Edwards, 1974).

A practical advantage of the MMR method over the previously mentioned total field methods is that it uses controlled sources. In all DC methods such as the MMR, very slowly varying currents are applied rather than static ones, for many reasons (explained below). This allow frequency domain filtering to obtain a high signal-to-noise ratio (Edwards, 1974).

The MMR method has not been a popular method because of the small magnitude of the anomalous magnetic field in large area surveys, and the practical difficulty of interpreting MMR anomalies. However, in small area surveys, the MMR method can potentially return strong enough signals by using today's highly sensitive magnetometers (see Section 9.b). Using numerical interpretation procedures, the MMR signals can be used to characterize unknown features. The methods have successfully been used to locate faults (Edwards, 1974) and for detection of ore bodies (Chen et al., 2002).

Near-surface applications:

For near surface applications, Edwards et al. (1978) studied a number of cases including buried faults, resistive/conductive buried river channels, and spheres. The method is potentially more useful in small area surveys where stronger signals can be obtained, and power of numerical modeling can be used for interpretations. The signal-to-noise ratio of the total magnetic field can be increased greatly using band-pass filters.

9.d. DC resistivity method:

In this method, (near) DC currents are applied using a pair of electrodes (denoted as points A and B below), and a second pair of electrodes is used to read the voltage difference at another two

points (M and N). Since the air is an insulating medium, all the energy dissipates into the lower half-space of the region. The array is designed such that the maximum amount of energy is returned to the receiver electrodes with the subsurface information.

The voltage difference as a function of applied current can be derived using the analogies in Table 6.1. That is, since the potential due to a current source is related to the inverse of the distance (i.e., 5.7), one can write the potential difference between M and N using the principle of superposition³

$$\begin{aligned}\Delta V_{MN} &= U_M - U_N = \frac{IR}{2\pi} \left(\frac{1}{r_{AM}} - \frac{1}{r_{BM}} \right) - \frac{IR}{2\pi} \left(\frac{1}{r_{AN}} - \frac{1}{r_{BN}} \right) \\ &= \frac{IR}{2\pi} \left(\frac{1}{r_{AM}} - \frac{1}{r_{BM}} - \frac{1}{r_{AN}} + \frac{1}{r_{BN}} \right)\end{aligned}\quad (9.12)$$

Here I represents the total applied current, and r_{XY} is the distance between electrodes X and Y. Then, the measured resistivity between points M and N is calculated to be

$$R = \frac{\Delta V_{MN}}{I} \frac{2\pi}{\left(\frac{1}{r_{AM}} - \frac{1}{r_{BM}} - \frac{1}{r_{AN}} + \frac{1}{r_{BN}} \right)} = \frac{\Delta V_{MN}}{I} K_g \quad (9.13)$$

Here K_g is a function only of the geometry of the measurement system and is called the *geometric factor* of the array.

The depth of penetration in DC methods can be estimated using a simple approach. Assuming a line separation of $2L$ between the current electrodes A and B, the current density at a depth z at the mid-point of AB is calculated to be

$$j(z) = \frac{IL}{\pi(L^2 + z^2)^{3/2}} \quad (9.14)$$

This formula gives an estimate of the current penetration with respect to depth. The current at depth z can be normalized using the magnitude of the current passing through the surface which is the maximum possible current. Then, one obtains a normalized current with depth as

$$\frac{j(z)}{j(0)} = \frac{1}{\left(1 + \left(\frac{z}{L} \right)^2 \right)^{3/2}} \quad (9.15)$$

The normalized currents as functions of depth are shown in Figure 9.5 for various electrode separation values. The curves show that the amount of current at some depth increases when the

³ Since the current is applied in the Earth in a half-space, which is bounded by an insulating surface on top, equations for the half-space model can be generated using “the method of images”. The resulting equations are identical to the whole space equations with a multiplication factor of 2.

separation of electrodes is increased. We note that for all curves, the effective depth of penetration (where the current suddenly drops) is around half of the distance between A and B. So the half-distance of the electrode separation is accepted as the depth of penetration in DC methods. One can also note that half of the current flows through the upper half of the total depth and the other half of the current flows beneath this.

In the DC methods, the current electrodes (A and B) and voltage electrodes (M and N) can be arranged in a number of different geometries. For different array geometries equation (9.13) is valid except the geometric factor (K_g) changes according to the type of array. These variations offer many different practical applications of the DC methods depending on the type of target being investigated. The two most widely preferred array designs are the Schlumberger and the dipole-dipole methods.

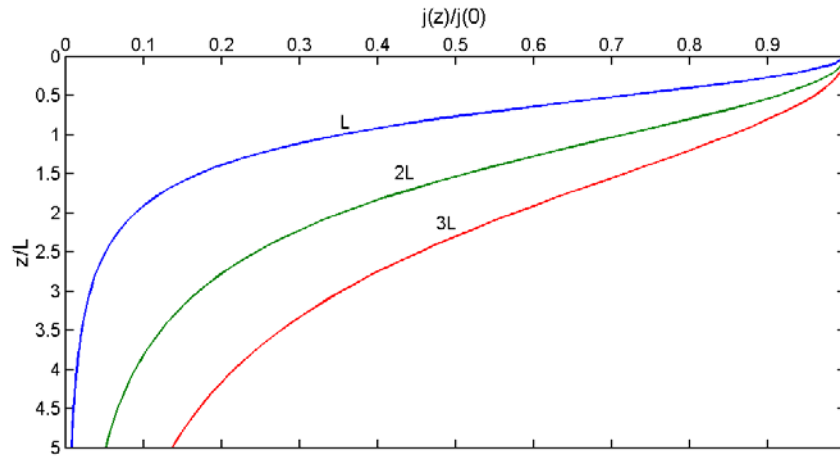


Figure 9.5 Current penetration in the DC method for various survey spreads

Schlumberger design:

In this configuration, all four electrodes lie along a line; current electrodes (A and B) are outside and the voltage electrodes (M and N) are inside, being symmetrical with respect to the midpoint of the survey spread. Distances between the measurement electrodes (MN) are kept small and constant during the measurement and the distance between outer (current) electrodes (A and B) is gradually increased. Because of the small distance of (MN), the measured voltage effectively gives the electric field at the center of AB. In a homogeneous and isotropic half-space, the geometric factor for the Schlumberger array by (3.7) is

$$K_g = \frac{\pi}{\left(\frac{1}{r_{AM}} - \frac{1}{r_{AN}} \right)} \tag{9.16}$$

The Schlumberger method is useful for small scale (shallow) surveys with dimensions up to 10 km.

Dipole-dipole design:

In this design, current injection electrodes (AB) and measurement electrodes (MN) are separated by large distances, so that the AB and MN distances become much smaller compared to the survey spread. This allows one to approximate the source (AB) as a single dipole source with

dipole moment \mathbf{p} which can be formulated as analogous to the electric dipole moment defined in Section 5.a (see equation 5.12):

$$\mathbf{p} = I\mathbf{d}_{AB} \quad (9.17)$$

Here we define vector \mathbf{d}_{AB} as the distance between point A to B; analogous to the separation between point electric charges in Section 5.a. The analogy in Table 6.1 between electrostatic and electric conduction can again be used to derive the equations for the dipole array, which by (5.14) yields the potential at the receiver distance

$$V_E = -\frac{R}{2\pi} \frac{\mathbf{p} \cdot \mathbf{r}}{r^2} \quad (9.18)$$

where \mathbf{r} represents the distance from the source to the measurement location and R represents the average resistivity of the medium. As in the case of the Schlumberger method, the measured potential difference can be approximated to electric field due to small MN separation. The measured electric field is represented by the electric field of a dipole source at some distance r (Zhdanov and Keller, 1994):

$$\mathbf{E} = -\nabla V_E = \frac{3R}{2\pi} \frac{\mathbf{p} \cdot \mathbf{r}}{r^3} \mathbf{r} - \frac{R}{2\pi r^3} \mathbf{p} \quad (9.19)$$

Dipole-dipole arrays are more practical for deep subsurface investigations (even studies related to crust scales) because these surveys do not demand cable connections between source and receiver arrays. However, the receiving signals are smaller in magnitude than in the case of Schlumberger arrays.

Near-surface applications:

DC resistivity methods are readily useful for two or three dimensional profiling of near-surface anomalies as a DC survey design must involve a finite source-receiver separation (The method is called by the acronym ERP for electrical resistivity profiling, as opposed to one-dimensional application named as VES for vertical resistivity sounding). Advantages of numerical modeling for ERP data can be done straightforwardly using the well-established theory of Maxwell equations and subsurface resistivities can readily be obtained in two or three dimensional space.

For detection of subsurface voids, the DC methods have been proven to be useful from theoretical perspectives (Spiegel et al., 1980; Munk and Sheets, 1997). Among various survey designs (i.e. Werner (see Parasnis, 1986), Schlumberger, and dipole-dipole arrays), dipole-dipole arrays have been shown to be by far the best method for detection of voids (Munk and Sheets, 1997; Zhou et al., 2002). A number of field studies (e.g., Zhou et al., 2002; El-Qady et al, 2005; Santos and Afanso, 2005; Leucci and De Giorgi, 2005; Ball et al., 2006) have used the dipole-dipole method to detect voids. In general, ERP has been a standard tool for detection of underground cavities (Dobecki and Upchurch, 2006).

10. Diffusive field methods

The main commonality of the diffusion methods is that the field diffuses into the medium from the surface. Therefore they are associated with an effective diffusion depth. Diffusion depth can be selected by two different ways: In *geometric sounding* (as in DC methods), the effective depth is a function of source-receiver separation; whereas in *parametric sounding* (as in the MT method), the effective depth is a function of the selected the frequency of the source. Both concepts are explained below.

10.a. MT method:

The atmosphere of the Earth is a very loose conductor whereas the Earth's subsurface has an electrical conductivity about 10 orders of magnitude larger. Consequently, electrical activities occurring in the atmosphere can easily penetrate into the Earth. This happens in two general ways; one as electromagnetic (EM) waves, and second, as transfer of electric charges. It was observed that the latter has a much smaller effect compared to the first one. The magneto-telluric (MT) method takes advantage of these penetrating EM waves, and returns us the subsurface electrical properties.

In the MT method, two general assumptions are made that the Earth has horizontally stratified electric properties ($R=R(z)$), and the atmospheric electromagnetic waves entering the Earth has a vertical direction of incidence. These assumptions greatly simplify the solution of the MT fields. As a result of this, the waves penetrating the Earth perpendicularly have non-zero amplitudes only in horizontal directions. Furthermore, due to the low frequencies of the waves, quasi-stationary form of the Maxwell equations (6.31-32) can be used (i.e., dielectric effects are neglected). Hence, the starting equation for the MT field is Helmholtz equations (6.26-27) in quasi-stationary form whose solutions can be represented one-dimensional plane waves (i.e., 5.43-44).

The depth of penetration or *skin depth* for the MT field can be defined as the depth at which the amplitude of the wave decreases by a factor of $1/e$. Then, for a horizontally layered Earth, the skin depth (δ_e) is calculated by

$$\frac{a(z)}{a(z + \delta_e)} = e^{2\pi\delta_e / \lambda} \quad (10.1)$$

Here, $a(z)$ represents the amplitude of waves at depth z . Using (6.35) we obtain

$$\delta_e = \frac{\lambda}{2\pi} \approx 0.159\lambda = 503.3(RT)^{1/2} \quad (10.2)$$

That is, the skin depth depends on the square-root of the resistivity and the wave period T (i.e. inverse of frequency). Equation (10.2) is the basic equation for parametric sounding in the MT method where the depth resolution is achieved by selecting different wave periods (i.e., parametric sounding).

In the plane wave solution of the MT fields, the ratio of the E -field to B -field is called the *wave impedance* (Z), i.e.,

$$Z_{xy} = \frac{E_x(z)}{H_y(z)} \quad \text{and} \quad Z_{yx} = -\frac{E_y(z)}{H_x(z)} \quad (10.3)$$

For an N -layered Earth with the last layer being a uniform half-space, the wave impedance is calculated to be (Zhdanov and Keller, 1994)

$$Z_{xy} = Z_{yx} = \frac{\omega\mu_0}{k_N} \quad \text{where} \quad k_N = \sqrt{\frac{i\omega\mu_0}{R_N}} \quad (10.4)$$

Note that the approximation ($\mu \sim \mu_0$) is made here for the reasons mentioned before. On the surface of the Earth ($z=0$) where the measurement is made, the impedance becomes

$$Z_{xy} = Z_{yx} = \frac{\omega\mu_0}{k_1} P_N. \quad (10.5)$$

Here, P_N is called the layered Earth correction factor. P_N takes simple forms for the two limiting cases of the conductivity of the last layer (i.e. N -th layer is a pure conductor or a pure resistor). The following values of Z can be obtained for the two limiting cases (Zhdanov and Keller, 1994):

For a perfectly insulating substratum with N rock layers on top:

$$Z = \frac{1}{S}, \quad \text{where} \quad S = \sigma_1 d_1 + \sigma_2 d_2 + \dots + \sigma_N d_N \quad (10.6)$$

For a perfectly conducting substratum with N rock layers on top:

$$Z = -i\omega\mu_0 D, \quad \text{where} \quad D = d_1 + d_2 + \dots + d_N \quad (10.7)$$

In equations (10.6) and (10.7), σ_i and d_i are the conductivity and thickness of the i th layer, respectively. By making proper frequency choices (using the skin depth, 10.2), either of these asymptotic equations can be used for N layers that are above the skin depth.

The power of the MT methods is that one has to measure only ratios of the E-field to the B-field on the surface (i.e., 10.3) in order to calculate the subsurface resistivities for N layers, and there is no need to try to correlate the amplitudes of the fields individually to the subsurface resistivities.

Unlike many other geophysical methods, it was shown that the MT method uniquely determines the electric properties of a horizontally layered Earth (Zhdanov and Keller, 1994). However, the uniqueness can be questioned when the Earth has a more complex structure than the assumed horizontality or when the noise in the actual data is considered.

Near-surface applications:

Frequencies used in the MT measurements are between 0.03 Hz and 250 Hz giving a depth range of 250 m to 3 km. For explorations purposes, high frequency waves are used; and the method is specifically called the audio-magnetotelluric method (AMT). The AMT method is extensively used in hydrologic and geothermal applications to locate the water bearing zones

down to a depth of a few km. The MT or AMT method seems to be not suitable for near-surface applications because of the requirement of using very high frequencies in order to resolve the shallow subsurface.

A specific type of electromagnetic method uses the very low frequency (VLF) waves (radio waves) that are generated by powerful distant man-made electromagnetic sources such as VLF signals from military bases or radio stations. It should be pointed out that although these radio waves are called VLF in their domain, they don't have low frequencies in the geophysical sense. These distant sources produce powerful E and B fields, which are near-horizontal at the far measurement locations but are still measurable. Although they are near horizontal they can easily penetrate into the Earth due to the much larger conductivity of the Earth compared to that of the air. By an approach similar to that of the MT method, the VLF source can be used for determining the electrical properties of the subsurface. In practice, the method is contingent upon a powerful source having a good signal-to-noise ratio.

10.b. EM/TEM induction method:

The electromagnetic (EM) induction method is similar to the MT method in terms of the application of the Maxwell equations that is in the quasi-stationary form so the \mathbf{E} and \mathbf{B} are treated as diffusing fields (see 6.31-32). However, the EM fields are different from the MT fields because their sources are generated artificially and are in the proximity of the measurement location; so the plane wave approximation is no longer valid.

Due to the strong source dependence of the EM induction method, it is also similar to the DC method. The difference is that, due to the existence of transient sources the time derivative of the electric and magnetic induction in the Maxwell equations (6.20-21) comes in to the equation, although all time-dependent terms are zero for stationary DC fields (6.45-48). The quantitative analyses of the EM method is generally more complicated, due to these two additional complexities compared to the MT and DC methods (i.e., proximity of the source to the receiver (unlike MT), and the transience of the source strength (unlike DC)).

In the EM method, the source consists of an electric current coil, which generates a transient magnetic field, called the *primary field*. As the primary field penetrates the Earth it causes generation of galvanic currents (eddies) due to the finite conductivities of the Earth materials. These induced currents generate induced magnetic fields, called *the secondary fields*. The secondary fields are measured on the surface using magnetometers, and these measurements can eventually be used to infer subsurface conductivities. One of the advantages of the EM method over other electrical methods is that neither the source nor the receiver requires surface penetration. On the other hand, in DC methods both source and receiver have to be in contact, and in the MT method the receiver has to be in contact with the subsurface. As a result of this, the EM (and TEM) method is superior to the former by being suitable for airborne deployment as well as allowing fast ground based surveys.

In the EM method, the subsurface electric properties can be obtained in various ways. In all of these ways, the basic approach is to compare the properties of the primary and secondary fields either in terms of changes in the directions (dip-angle methods) or changes in phases (phase shift methods) of the secondary fields (Parasnis, 1986). (In practice, there are also many variations of these two basic approaches but they will not be discussed here.) The advantage of the dip-angle method is that the direction of the secondary field is a function of the attitude of the subsurface anomaly, giving a structural constraint. However, due to limited accuracies in the determinations of both the primary and the secondary fields, the dip-angle method is not suitable for quantitative applications; and they are better suited for reconnaissance studies.

Phase shift methods use the notion of impedance of the rocks (10.4), which is a complex number. The secondary waves experience a phase shift depending on the impedance of the rocks, which can eventually be used for resistivity determination. The advantage of the phase shift method is that the measurement is independent of the orientation of the fields; which makes the method more appropriate for quantitative analyses.

In the EM method, depth penetration can be done either geometrically by parameterizing the transmitter-receiver separation (as in the DC method); or parametrically by using different source frequencies (as in the MT method). The latter has the advantage of using one set of sensors as both transmitter and receiver, and is suitable for airborne applications.

The magnitude of the measured field (secondary field) in the EM method totally depends on the conductivity of the subsurface layers; the returning signal is zero if the subsurface is an insulator. Earth materials are poor conductors; so the amplitudes of the secondary fields are generally very small unless there is a highly conducting anomaly in the subsurface such as a metal ore body. As a result of this, the best applications of the EM method are found in mineral explorations and metal detection (such as UXO; Bell et al., 2001).

In the EM method, only monochromatic waves are used in order to have a better frequency filtering. A wide range of frequencies can be used from a few Hz to a few KHz, which makes the method applicable down to 500 m. In airborne surveys, frequencies are higher (> 400 Hz), and are generally designed for detecting shallow conductive anomalies (i.e., geological reconnaissance mapping).

TEM method:

In the continuous EM method (above), constant frequency waves are used as the source, which also requires a constant energy source in practice. In the transient electromagnetic (TEM) method, the primary field is applied for a limited amount of time in the form of a pulse, and the secondary field is measured after the primary field is shut off. Since the primary field is a pulse in time domain it leads to generation of a wide frequency spectrum in frequency domain. Due to this nature, the TEM data is usually analyzed in the frequency domain⁴. The TEM method is practically advantageous since less power is needed compared to the continuous EM method.

In fact, the advantages of the TEM method go beyond practical considerations. That is, low frequency primary fields (less than a Hz) are very hard to generate using the continuous EM method, which puts a depth limitation on its applicability (less than 500 m). On the other hand, very low frequencies are easily generated with the TEM method, which makes it suitable for depths up to 10 km.

The inability to pre-determine frequencies in the TEM method prohibits frequency parameterization for depth determination. This problem can be overcome by time parameterization in the TEM method. That is, since the quasi-stationary Maxwell equations represent diffusing fields (6.31-32), then a *diffusion depth* can be introduced for the TEM fields analogously to the notion of a *skin depth* in the EM. The diffusion depth for the TEM method is then defined as

$$\delta = 503.3\sqrt{tR} \quad (10.8)$$

⁴ The former method (continuous EM), which uses a single pulse of frequency, is sometimes called the frequency domain electromagnetic (FDEM) method for being complimentary to the time-domain electromagnetic (TEM/TDEM) method here where a pulse in time is used.

Here, R is the average resistivity of the medium, and the parameter t is the total time of measurement after the system is turned off; so a longer delay in time of the measurement refers to information from deeper parts of the subsurface.

Near surface applications:

The EM/TEM methods work best for conductive anomalies such as in the detection of UXO's (Bell et al., 2002; Butler et al., 2006) and metal ores. They are also very useful for mapping very shallow (<10m) conductivity variations. Due to the additional fact that EM/TEM surveys can be made efficiently using airborne sensors, the method is extremely useful in geologic mapping, especially in inaccessible areas.

There have been cases of the EM/TEM method for detection of underground cavities. Witten (2006) presented a number of examples of TEM studies over tunnels and archeological sites. The results are satisfactory but not conclusive unless supported by *a priori* knowledge. Ball et al. (2006) used the TEM method over an archeological site in New Mexico, along with other DC electric methods. However, their purpose of using TEM was to understand the electric conductivity of the background structures rather than detecting the cavities. Their results show that TEM data provide good resolution at shallow depth but very poor resolution below the shallow overburden. As a result, the EM/TEM methods appear to be less useful for detection of cavities compared to other electrical methods. However, practicality of the EM/TEM method makes it attractive for using in a variety of fields for obtaining auxiliary information.

10.c. IP method:

For a constant amount of voltage applied into the Earth's subsurface, the electrical behavior of the rocks can be approximated as that of simple resistors. However, at the same time, a finite amount of charge accumulation also emerges at mineral boundaries as a result of differences in electrical properties. The induced polarization (IP) is different from the polarization concept discussed in Section 6a where the latter occurs at atomic or molecular scales whereas IP phenomenon is totally a macroscopic event as a result of electrical discontinuities of Earth materials (Zhdanov and Keller, 1994).

In all DC applications, the effect of IP also exists but the voltage associated with IP is negligibly small compared to the applied voltages, so IP effects are ignored. However, IP manifests itself as a finite amount of decaying voltage reverse direction as the DC source is shut off. During this stage, effective dielectric constants are some 5 orders of magnitude larger than the normal dielectric constants of rocks, and the resulting stored energy is dissipated into the environment. At the IP stage, rocks can be treated as resistor-capacitor (RC) pairs with frequency dependant impedances. Because of this, it is more appropriate to analyze the IP phenomenon in the frequency domain. In the IP method, one measures two IP resistivities for two frequency values; one with low (mHz range) frequency, and one with high (in Hz range) frequency. In modeling the IP, one uses the apparent resistivities determined at these two frequencies, and calculates a parameter known as *apparent polarizability* (η_a) of the medium by (Zhdanov and Keller, 1994)

$$\eta_a = \frac{R_a^l - R_a^h}{R_a^l} = \frac{1}{R_a^l} \frac{\partial R_a^l}{\partial \omega} \Delta\omega \tag{10.9}$$

Here, ω represents the frequency, and R_a^l and R_a^h are the apparent resistivities at the two selected low and high frequencies, respectively. The choice of the low frequency for the purpose of normalization is arbitrary.

Although modeling of IP in a complex geological scheme is generally complicated, the apparent polarizability for a simple example of two resistive mediums with resistivity values of R_1 and R_2 can be modeled rather easily. For simplicity we assume that only one medium has a polarizability (η) and the other medium is not polarizable. Then, the apparent polarizability (η_a) is calculated by

$$\frac{\eta_a}{\eta} = \frac{(1 - K_{12}^2)}{2R_a} \frac{\partial R_a}{\partial K_{12}} \quad \text{where } K_{12} = \frac{(R_2 - R_1)}{(R_2 + R_1)}. \quad (10.10)$$

Here, K_{12} is called the *Kelvin reflection factor* looking from medium 1. Equation (10.10) is a very useful formula to investigate the effects of IP. It also relates the apparent resistivity (R_a) to apparent polarizability (η_a). In fact, one can observe that IP anomalies resemble resistivity anomalies in field measurements (Zhdanov and Keller, 1994). It can be shown using (10.10) that conductive anomalies generate higher IP signals than resistive anomalies. Finally, for the limiting case of infinite resistivity (i.e., voids, $R_1 = \infty$), no IP anomaly exists. Nevertheless, the IP method is an ideal procedure in locating ore deposits due to the fact that it returns a strong response from conductors and also that, compared to DC methods, it requires less power in the field.

A polarization similar to the IP phenomenon can naturally occur in the subsurface by the interaction of subsurface conductors with the surrounding rocks in a rather complicated way. These are called SP (spontaneous polarization) anomalies and are sometimes used to detect subsurface conductors. Porous sandstone formations, which can host oil/gas deposits, and SP method is frequently used for geophysical logging of oil/gas wells during development.

10.d. SASW method:

When seismic body waves (P and S waves) hit a free medium on the surface of the Earth they turn into surface waves. P waves (along with the vertical component of S waves) produce *Rayleigh waves*; whereas S waves (the horizontal component) turn into *Love waves* (Figure 10.1). As a result of this, Rayleigh waves produce vertical surface displacement, whereas Love waves produce horizontal movements (Figure 10.1). Amplitudes of surface waves attenuate by square-root of distance whereas body waves attenuate linearly by the distance. As a result of this, surface wave (especially Love waves) generated by earthquakes cause most of the destruction in built-up areas (Van der Hilst, 2004).

In exploration seismology, surface seismic waves are generally considered as noise to be removed (i.e., in refraction and reflection seismology) because they carry only information of the shallow subsurface. However, in near surface applications they turn out to be useful. Since artificial seismic sources mainly produce P -waves, they lead to generation of high amplitude Rayleigh waves which are used in surface wave studies (Park et al., 1999).

The amplitudes of surface waves decay exponentially with depth and their effective depth is in the order of $\sim \lambda/3$, where λ is the wavelength (Van der Hilst, 2004). Since the waves with varying frequencies experience different effective thicknesses (and therefore different effective elastic properties), surface waves are subject to dispersion. It is this dispersive nature of surface waves that is used for subsurface characterization. Using multi-channel receiver deployment,

spectral analysis of surface waves (SASW) can be used to obtain the shallow subsurface elastic properties (Park et al., 1999).

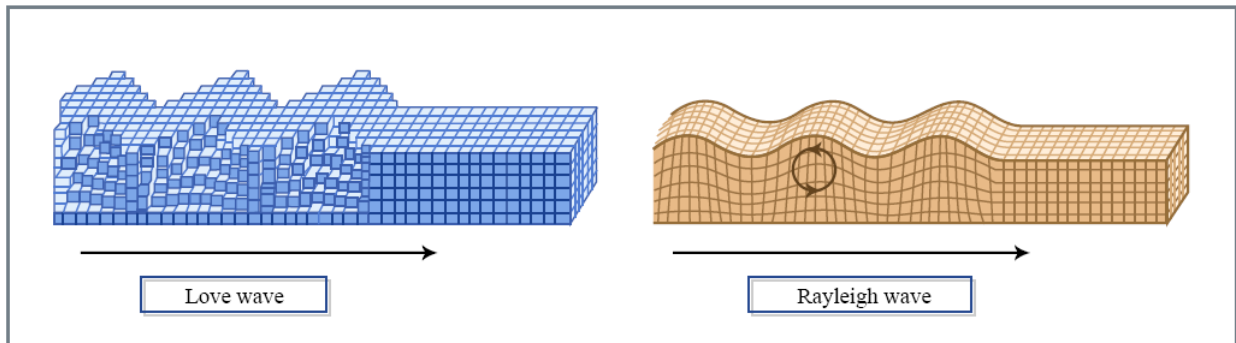


Figure 10.1 Types of surface seismic waves (Van der Hilst, 2004)

Dispersion of surface waves has been employed for detection of shallow voids using frequency (Cull et al., 2005) and time domain (Xia et al., 2007) analyses. In fact, interaction of surface waves with subsurface cavities is a complex problem as a result of reflection, diffraction and attenuation of the surface waves over the cavity. Nasseri-Moghaddam et al. (2005) numerically showed that the horizontal location of a cavity can be determined by studying the changes in the group velocity of the Rayleigh wave in the time domain, and the vertical location of the cavity can be detected in the frequency domain by studying the attenuated frequencies. However, they did not present field examples to test the validity of their model. On the other hand, Grandjean and Leparoux (2004) reported results of an experimental field test, and concluded that cultural noise may impose important limitations on the application of surface waves for cavity detection (and on seismic methods, in general, see below). This may be the underlying reason for the relatively larger amount of published numerical studies of surface waves for detecting cavities compared to the fewer demonstrations for actual field results.

11. Transient field methods

The basic principle of the transient field methods is that they can be studied within the context of the ray theory since the fields act as true waves (Van Der Hilst, 2004). These methods can be studied in two broad categories based on refractive (seismic refraction) and reflective properties of the rays (GPR and seismic reflection). In (seismic) refraction methods, a signal is sent to the subsurface from one source and the refracted signal is received at some distance (survey spread). The returning signal carries information of the media through which it passes. The depth from which information is returned to the surface depends on the offset between the source and the receiver; a larger spread resolves deeper layers (geometric sounding, explained before). In the refraction method, one is interested in the internal physical properties of the medium through which the rays are passing. As a result, information carried by the ray is a space averaged physical property of the subsurface.

On the other hand, the general working objective of the reflection methods (e.g. GPR, and seismic reflection) is to detect the reflected signals from discontinuities in the subsurface. As in the case of refraction methods, the ray theory also applies in the treatment of reflection methods.

Since reflected signals are sensitive to the contrasts across mediums rather than internal properties of the mediums, unlike the refraction methods, the internal properties are not resolved

in these methods. As a result, reflection methods work as “imaging” tools for the subsurface structure.

11.a. Seismic refraction method:

When a seismic wave hits an elastic boundary, critically refracted waves travel along the boundary with the speed of the lower medium but they also excite the particles at the top medium as they travel (Van Der Hilst, 2004). These continuously generated secondary waves (head waves) reach the surface with the same incidence angles of the original wave. The travel times of the waves reaching the surface carry the information of the velocities of the refracting layer as well as information of all overlying layers.

The basic rationale that the seismic refraction method is applicable comes from a fundamental physical property of the Earth. That is, according to Snell’s law of ray theory (Van Der Hilst, 2004), for a seismic ray to return to the surface, seismic velocities of rocks should increase with depth. Fortunately, this condition is met for most of the cases of Earth systems, and input seismic waves can return subsurface information to the surface.

In refraction studies the primary interest is the velocity structure of the subsurface media; so the resulting models are primarily used to predict internal elastic properties. As discussed below, this is not the case for reflection seismology since its primary interest is detecting discontinuities. The refraction method can be used in small area applications (such as basin analysis) or for large scale crustal studies. In tectonic studies, it is the preferred active source seismic method for determination of Moho undulations.

Near-surface applications:

The most widely used shallow applications of the seismic reflection method are in the determination of the depth to bedrock in site investigations (McCann et al., 1987). For detection of subsurface cavities, a number of studies have noted that the seismic refraction method is not feasible (e.g., McCann et al, 1987; Munk and Sheets, 1997). From the theoretical perspective, as mentioned above, the main requirement of seismic reflection is an increase in velocities with depth. However, this condition is not met for subsurface cavities as they have lower velocities with respect to their overlying mass. As a result of this, a subsurface cavity does not lead to critical refraction of seismic signals (Munk and Sheets, 1997). From a practical perspective, high frequency body waves are required for detection of cavities; but they are prone to fast attenuation resulting in low signal-to-noise ratio. On the other hand, lower frequency signals are unable to resolve the cavities (Greenfield et al, 1976). In general, these problems are more severe in places with high cultural noise (Grandjean and Leparoux, 2004).

11.b. GPR method:

We previously mentioned that certain approximations are made in the Maxwell equations in different frequency ranges. We stated that at very high frequencies (e.g., > 1 MHz for geophysical applications) the first time derivatives in the telegrapher’s equations (5.26-27) become small compared to the second time derivatives, and the \mathbf{E} and \mathbf{B} fields can be represented by wave equations (6.36-37). Under these conditions, the fields are said to propagate by radiation (Section 6.b). Since conductive properties of rocks are not relevant for the behavior of the waves, it is convenient to set $\mathbf{j}=0$ in the Maxwell equations (6.9-12). However, finite conductivity of the medium still plays role in the determination of the electrical properties of the medium, which has a specific name at this stage: *lossy dielectric medium*. It is characterized by a complex dielectric

permittivity stated in terms of a function of both dielectric constant and the electrical conductivity:

$$\varepsilon^* = \varepsilon + i\sigma / \omega \quad (11.1)$$

In passing a boundary with different dielectric properties, the waves are both reflected and refracted following Snell's law for electromagnetic radiation (Zhdanov and Keller, 1994):

$$\frac{\sin \phi_1}{\sin \phi_2} = \sqrt{\frac{\varepsilon_2^*}{\varepsilon_1^*}} \quad (11.2)$$

Thus, the waves are responsive to changes in both dielectric and conductive properties of the subsurface units. In the GPR, using a pair of antennas for source and receiver, one can measure the time delay between the incident and reflected wave and convert it into depth using the velocity of the radiating waves inside the dielectric medium, which is given by

$$c' = \frac{1}{\sqrt{\varepsilon\mu}} \quad (11.3)$$

So, as mentioned before, the aim of GPR is detecting the electrical contrast between different mediums rather than determining the internal electrical properties of the media. The amplitude of the reflected signal depends on various parameters, which are represented by the *radar equation* as follows

$$P_r = P_t K_{g1} K_{g2} F_t A_r L_{p1} L_{p2} \quad (11.4)$$

P_r : Power returned to the radar

P_t : Power of the transmitter

K_{g1} : Reduction in the power density at the front of the radiating field caused by geometric spreading

K_{g2} : Reduction in the power density at the front of the reflected field

F_t : Reflectivity of the target

A_r : Effective area of the receiving antenna

L_{p1} : Attenuation of the radiating field in the lossy medium

L_{p2} : Attenuation of the reflected field in the lossy medium

Among these parameters the reflectivity of the target (F_t) depends on the electric properties of the target, whereas the others are generally related to the properties of the background medium. Assuming that the magnetic properties are similar, the reflectivity of an interface between two mediums looking from medium 1 can be calculated, using equation (11.3), as

$$F_t = \frac{c_2' - c_1'}{c_2' + c_1'} = \frac{\sqrt{\eta_2} - \sqrt{\eta_1}}{\sqrt{\eta_2} + \sqrt{\eta_1}} \quad (11.5)$$

where η represents the dielectric constant of a particular medium as defined in (6.4). We note that the assumption of constant magnetic permeability may not be valid for rock-metal interfaces. Using Table 8.1, reflection coefficients can be calculated for various subsurface anomalies. For a background consisting of rocks, the highest reflections are generated from metals ($\eta_2 > 70$). For subsurface voids ($\eta_2 = 1$), the reflection coefficient has negative values implying that the amplitudes of the reflected waves are reversed, which is also true for all insulating anomalies.

The effective depth of penetration (δ_e , see equation 10.1) in the GPR depends on both the resistivity (R) and the dielectric constant (η) of the medium by the following equation (Owen, 1995):

$$\delta_e \approx 5.3 \times 10^{-3} R \sqrt{\eta} \quad (11.6)$$

In an insulating medium, the depth of penetration can be as deep as 50 m. However, existence of water inside the rocks limits most of the GPR applications to shallower depths (< 20 m) (Knight, 2001). As a rule of thumb, mediums with resistivities below 100 Ω -m are not practical for the GPR method.

Near surface applications:

All applications of the GPR method are for the near surface region because of the limitations in depth of penetration of radiating EM waves. The foremost important parameter for an efficient GPR survey is the electric resistivity of the medium. Another factor is the contrast between electric resistivities of the target and the host medium. If these conditions are right, the GPR method becomes a very easy and effective tool for imaging near-surface anomalies because of it is a non-destructive and rapid measurement technique.

GPR is expected to respond to a subsurface cavity as a result of the large resistivity contrast between the void and the host medium (Glover, 1992). The GPR method has been widely used for detection of underground cavities (Dobecki and Upchurch, 2004). Many successful field examples of GPR for detection of voids have been reported in combination with other geophysical methods, such as GPR and DC resistivity (Leucci and De Giorgi, 2005; El-Qady et al., 2005), and GPR and gravity (Beres et al., 2001; Mochales et al., 2008). Under favorable conditions, a GPR image can give both location and the depth of a void. One of the practical obstacles of the GPR method is that objects above the surface are seen as buried objects (similar to the signal of a void) in addition to subsurface anomalies. To solve this problem, a shielded GPR tool can be used to filter certain frequencies reflected from above the ground. Munk and Sheets (1997) compared GPR measurements at three different sites for the detection of cavities; and showed dramatic effects from above-surface features and high conductivity subsurface environments on the GPR signals.

Since GPR measurements are made with small source-receiver separation, the resulting models are inherently one-dimensional. This results in the distortion of localized anomalies in the radar image. So, a special numerical processing called “migration” has to be applied in order to obtain the physical image (Beres et al., 2001). A direct method for obtaining two dimensional GPR images has been developed recently. The method uses the principle of synthetic aperture radar (SAR) imagery, which is commonly used for topographic modeling by airborne and spaceborne radar sensors. In this method (called GPR-SAR), the GPR reflection signals are retrieved from two different angles and are merged for focusing the target in its true or three dimensional location. Preliminary field test results of GPR-SAR are given by (Kazunori, 2006).

Recently, the method has been proposed for the Japanese lunar radar sounder (LRS) radar SELENE to image the near-surface faults of the Moon from space (Kobayashi and Ono, 2007).

11.c. Seismic reflection method:

As the two primary reflection methods in geophysical applications, ground penetrating radar (GPR) and seismic reflection have great similarities in their working principles; except the former uses EM waves, whereas the latter uses acoustic waves. Since propagation speeds of these two types of waves are greatly different, the former works in nanosecond time scales, whereas the latter uses millisecond time scales. Other than that, the two methods are identical in terms of working principles.

The principle of the ray theory applies in the seismic reflection method as well, but in this case one is interested in the reflected waves from an elastic interface rather than an electrical one. The amplitude of the reflected wave from an interface is related to the contrast in the acoustic impedance, which is defined as the density times the velocity (Lillie, 1999). The reflection coefficient for the reflected wave (looking from medium 1) can be formulated as

$$F_s = \frac{\rho_2 v_2 - \rho_1 v_1}{\rho_2 v_2 + \rho_1 v_1} = \frac{Z_2 - Z_1}{Z_2 + Z_1} \quad (11.7)$$

where Z is called as the *acoustic impedance* in analogy with the *wave impedance* in electromagnetism (i.e., 10.4). Unlike the seismic refraction, the seismic reflection method does not pose any restriction of increase in seismic velocities with depth. As seen in (11.7), the only requirement for obtaining a reflection signal ($F_s \neq 0$) is the contrast in the acoustic impedances between the two mediums.

The reflection methods work best for relatively deep structural discontinuities as the acoustic impedances of shallow (<0.1 km) reflectors are generally weak. The depth of illumination is limited by the attenuation of seismic energy which depends on the size of the source and initially generated frequency ranges. In reflection methods, typical depths of interests are less 10 km.

As in the case of GPR method, the principle quantity that seismic rays seeing is the change in the elastic properties rather than internal elastic properties of the mediums. The amount of energy reflected from an interface is related to the acoustic impedance of the rocks.

In the reflection seismology, typical frequencies are in the order of 10-100 Hz, which can resolve structures of 30-300 m in size. In order to resolve both small and large scale structures, a wide frequency band (near delta function spikes) source is required.

Near-surface applications:

Near-surface applications of seismic reflection (particularly in detection of cavities) are limited for similar reasons mentioned above for the seismic refraction method. That is, high frequency signals which are required for detection of small anomalies quickly attenuate in the subsurface giving very low quality signals (Greenfield et al., 1976). As a result of this, seismic reflection methods do not have applications in detection of subsurface cavities.

12. Discussion

In the previous sections, we grouped the geophysical methods by their geometrical and mathematical similarities rather than with respect to their fundamental physical similarities.

Admittedly, the categorization of the methods is a “non-unique” problem; that is, a method may resemble to one from one side but it may resemble to a different method from another side. Nevertheless, the present effort is to find an optimal way to show outstanding analogies with basic principles.

Among the geophysical methods discussed above, electrical methods have by far the largest diversity in their applications. So, in the next section, a side-by-side comparison of these methods is given in terms of certain parameters.

12.a. Comparison of the electrical methods

In all electrical methods described above, various forms of the Maxwell equations were applied according to the selection of the source frequency. Table 12.1 shows a comparative summary of the electric methods used in geophysical applications.

Table 12.1 A comparison of electrical methods

	Frequency range	Responsive units	Field Behavior	Effective parameter	Practical depths
DC	N/A	Resistive	Stationary	σ	< 300 m
IP	N/A	Both	Stationary	σ	< 300 m
MMR	N/A	Both	Stationary	σ	< 100 m
EM	1 Hz - 100 KHz	Conductive	Quasi-stationary	σ	< 5 km
TEM	10 mHz - 100 KHz	Conductive	Quasi-stationary	σ	< 10 km
MT	1 mHz - 100 KHz	Both	Quasi-stationary	σ	0.1- 100 km
GPR	10 MHz - 1000 MHz	Both	Radiation	ϵ, σ	< 20 m

The main characteristic of the methods depends on the frequency ranges used. In DC methods, the source current is ideally constant. However, it is more practical to use very slowly varying currents (i.e., very low frequencies) in order to remove the effect of charge accumulation between electrodes and the ground. In DC methods, most of the electric energy is taken by the resistive layers, so these methods are more responsive to resistive anomalies.

At low frequencies (less than a MHz), the diffusion form of the EM fields (including EM, TEM and MT) is used where diffusive behavior (quasi-stationary form) of the fields dominates. In this form the dielectric properties of the Earth (so, the displacement currents) are not significant. Unlike the DC method, EM/TEM methods work best for conductive anomalies as these methods use the principle of electromagnetic induction of conductors. Using the complementary behavior of the DC and EM methods, i.e., the former being responsive to resistive layers, whereas the latter being responsive to conductive layers, Raiche et al., (1985) used a combined interpretation procedure of both methods to improve the resolution of electrical inversions.

At high-frequencies (above MHz), the electromagnetic fields act as true waves in the Earth and the radiation forms of Maxwell’s equations are applied. In this state, the dielectric properties of the medium dominate over the conductive properties in the behavior of the EM field. Earth’s conductivity only comes into the formulas in order to study the attenuation of the EM waves within the medium. In GPR, one uses the reflective properties of EM waves across material boundaries, which is a function of the contrast in dielectric (and magnetic) properties. As a result of this, the GPR method finds applications for both high and low dielectric anomalies. Due to fast attenuation of waves at high frequencies, the GPR method is limited to very shallow applications.

12.b. Relevance of methods to void detection

We already discussed the feasibility of each geophysical method for applications on cavities at the end of the discussion of each method. It should be apparent so far that some methods are more suitable than others for detection of subsurface cavities.

In the total field methods, gravity seems to be the best method for void detection (and is likely one of the best methods among the entirety of geophysical methods) due to large gravity contrast between the void and the host medium. Magnetic methods also seem to be applicable as a result of high sensitivities of magnetic field sensors, so even a small contrast in magnetic properties between the void and the host medium can potentially be detected. MMR has not been used for cavity detection so far; but this method can potentially be useful for detection of voids due to number advantages over other electrical methods discussed so far.

Among electrical methods DC resistivity and GPR stand out as the two best methods for detection of cavities. DC methods are readily useful for near surface applications (including detection of cavities) because they use the concept of geometric spreading (profiling), and two or three dimensional Earth model are already assumed. This is useful for near-surface applications because the horizontal and vertical dimensions of anomalies are comparable in size. By profiling, subsurface anomalies can be straightforwardly identified at their exact locations. Among various array designs, both numerical and field examples show that the dipole-dipole design gives by far the best response to subsurface voids. The GPR method is also useful in void detection as it responds to cavities at the air-rock boundary. The GPR method inherently uses a one-dimensional Earth model, but spatially distributed 1-D signals can be processed to retrieve the 2-D Earth structure (generally called as *migration* process). GPR is a common geophysical tool for void detection because of its practicality as well as the responsiveness to subsurface voids. The basic limitation of the GPR method is that, for highly electrically conductive mediums, the results are not satisfactory as the EM waves attenuate before reaching the target depths.

Body wave seismic methods (reflection and refraction) seem to be not useful for void detection as high seismic frequencies needed for the detection are greatly attenuated within short distances, leaving a low signal-to-noise ratio for the void. Surface wave seismic methods have also been studied for void detection. However, controlled field experiments only show marginal promise, and successful field studies are very few as a result of cultural noise.

References:

- Ball L.B., J.E. Lucius, L.A. Land, and A.P. Teeple (2006), Characterization of Near-Surface Geology and Possible Voids Using Resistivity and Electromagnetic Methods at the Gran Quivira Unit of Salinas Pueblo Missions National Monument, Central New Mexico, June 2005, *USGS, Scientific Investigations Report 2006–5176*.
- Baranov, V. (1957), A new method for interpretation of aeromagnetic maps: Pseudo-gravimetric anomalies, *Geophysics*, 22, 359-383.
- Baranov V. (1975), *Potential Fields and Their Transformations in Applied Geophysics*, Gebrüder Borntraeger, Berlin.
- Bell, T.H., B. J. Barrow, and J. T. Miller (2001), Subsurface discrimination using electromagnetic induction sensors, *IEEE Transactions on Geoscience and remote sensing*, 39, 1286-1293
- Beres, M., M. Luetscher, R. Olivier (2001), Integration of ground-penetrating radar and microgravimetric methods to map shallow caves, *Journal of Applied Geophysics*, 46, 249-262.
- Butler, R. F. (1992), *Paleomagnetism: Magnetic domains to geological terranes*, Blackwell Scientific Publications, Boston.
- Chapin, D.A., M.F. Crawford, and M. Baumeister (1999), A side-by-side test of four land gravimeters, *Geophysics*, 64, 765-775.
- Butler, D.K., H. H. Bennet, and J. H. Ballard, Overview of multi-method geophysical system development for enhanced near-surface target detection, discrimination, and characterization, *The Leading Edge*, 25, 352-356.
- Chen, J., E. Haber, and D.W. Oldenburg (2002), Three-dimensional numerical modeling inversion of magnetometric resistivity data, *Geophysical Journal International*, 149, 679-697.
- Clark, S. P. (Editor) (1966), *Handbook of Physical Constants*, Geological Society of America Memoir 97, Revised edition, New York.
- Cook, J.C., and S. L. Carts (1962), Magnetic effects and properties of typical topsoils, *Journal of Geophysical Research*, 67, 815-828.
- Cull, J., G. Jung, and D. Massie (2005), Cavity detection using single-fold frequency analysis, *Journal of Environmental and Engineering Geophysics*, 10, p. 80-81, doi: 10.2113/JEEG10.2.80.
- Edwards, R. N., (1974), The magnetometric resistivity method and its applications to the mapping of a fault, *Canadian Journal of Earth Sciences*, 11, 1136-1156.

- Edwards, R.N., H. Lee, and M.N. Nabighian (1978), On the theory of magnetometric resistivity (MMR) methods, *Geophysics*, 43, 1176-1203.
- El-Qady, G., M. Hafez, M.A. Abdalla, and K. Ushijima (2005), Imaging subsurface cavities using geoelectric tomography and ground penetrating radar, *Journal of Cave and Carst Studies*, 67, No 3, 174-181.
- Dobecki, T.L., S.B. Upchurch (2006), Geophysical applications to detect sinkholes and ground subsidence, *The Leading Edge*, 25, 336-341.
- Glover J.M. (1992), Void detection using standing wave analysis, *Paper by Geological Society of Canada*, 1992, 63-73.
- Grant F.S., and G.F. West (1965), *Interpretation Theory in Applied Geophysics*, McGraw-Hill Book Company, New York.
- Grandjean, G., and D. Leparoux (2004), The potential of seismic methods for detecting cavities and buried objects: experimentation at a test site, *Journal of Applied Geophysics*, 56, 93–106.
- Greenfield, R.J., P.M. Lavin, and R.R. Parizek (1976), Geophysical methods for location of voids and caves, *Publication of the International Association of Hydrological Sciences Proceedings of the Anaheim Symposium*, December 1976, 465-484.
- Hansen, R.O. (2001), Gravity and Magnetic methods at the turn of the millennium, *Geophysics*, 66, 36-37.
- Hofmann-Wellenhof, B., Moritz, H. (2005): *Physical Geodesy*. Springer, Wien.
- Jekeli, C. (1987), New Instrumentations techniques in geodesy, *Reviews of Geophysics*, 25, 889-894.
- Jekeli, C. (2000), *Inertial Navigation Systems with Geodetic Applications*, Walter de Gruyter, Berlin.
- Jekeli, C. (2004): High-Resolution Gravity Mapping: The Next Generation of Sensors. In: R.S.J. Sparks (ed.), *The State of the Planet: Frontiers and Challenges in Geophysics*, Geophysical Monograph 150, IUGG vol.19, 135-146.
- Jekeli, C. (2007), Potential theory and static gravity field of the Earth, *Treatise on Geophysics V.3*, Herring, T. (Ed.), 11-42.
- Jekeli, C. and J.H. Kwon (1999), Results of airborne vector (3-D) gravimetry, *Geophysical Research Letters*, 26, 3533-3536.
- Kaula, W. M., (1966), *Theory of Satellite Geodesy*, Waltham, Blaisdell.

- Knight, R. (2001), Ground penetrating radar for environmental applications, *Annual Review of Earth Planetary Sciences*, 29, 229-255.
- Kobayashi, T. and T. Ono (2007), SAR/InSAR observation by an HF sounder, *Journal of Geophysical Research*, 112, E03S90, doi: 10.1029/2005JE002576.
- Leucci, G., and L. De Giorgi (2005), integrated geophysical surveys to asses the structural conditions of a karstic cave of archeological importance, *Natural Hazards and Earth System Sciences*, 5, 17-22.
- Li, X, and C. Jekeli (2008), Ground-vehicle INS/GPS vector gravimetry, *Geophysics*, 73, I1-I10, doi: 10.1190/1.2821155.
- Lillie, R.J. (1999), *Whole Earth Geophysics*, Prentice-Hall Inc., New Jersey.
- Menke, W., and Abbott D. (1990), *Geophysical Theory*, Columbia University Press, New York.
- McCann, D.M., P.D. Jackson, and M.G. Culshaw (1987), The use of geophysical methods in the detection of natural cavities, *Quarterly Journal of Engineering Geology*, 20, 59-73.
- McGrath, R.J., P. Styles, E. Thomas, S. Neale (2002), Integrated high-resolution geophysical investigations as potential tools for water resource investigation in karst terrain, *Environmental Geology*, 42, 552-557.
- Mochales, T., A.M. Casas, E.L. Pueyo, O. Pueyo, M.T. Romàn, A. Pacovì, M.A. Soriano, D. Anson (2008), Detection of underground cavities by combining gravity, magnetic and ground penetrating radar surveys: a case study from the Zaragoza area, NE Spain, *Environmental Geology*, 53, 1067-1077.
- Munk, J., and R.A. Sheets (1997), Detection of underground voids in Ohio by use of Geophysical methods, *U.S. Geological Survey*, Water-Resources investigations report 97-4221.
- Nasseri-Noghaddam, A., G. Cascante, and J. Hutchinson (2005), A new quantitative procedure to determine the location and embedment depth of a void using surface waves, *Journal of Environmental and Engineering Geophysics*, 10, 51-64.
- NRC (1997), *Satellite gravity and the geosphere*, National Academy Press, Washington, DC.
- Owen, T.E. (Ed) (1995), Ground penetrating radar, *Journal of Applied Geophysics*, 33(1-3), 1-225.
- Parasnis, D.S. (1986), *Principles of Applied Geophysics*, 4th Ed., Chapman and Hall, , New York.
- Raiche, A.P., D.L.B Jupp, H. Rutter, and K Vozoff (1985), The joint use of coincident loop transient electromagnetic and Schlumberger sounding to resolve layered structure, *Geophysics*, 50, 1618-1627.

- Park, C.B., Miller R.D., J. Xia (1999), Detection of near surface voids using surface wave, *Kansas Geological Survey, Open file report PAR-99-01*.
- Riley, K.F., M.P. Hobson, and S.J. Bence (1997), *Mathematical Methods for Physics and Engineering*, Cambridge University Press, Cambridge.
- Romaides, A.J., J.C. Battis, R.W. Sands, A. Zorn, D.O. Benson Jr., and D.J. DiFrancesco (2001), A comparison of gravimetric techniques for measuring subsurface void signals, *Journal of Physics D: Applied Physics*, 34, 433-443.
- Rummel R., G. Balmino, J. Johannessen, P. Visser, and P. Woodworth (2002), Dedicated gravity field missions-principles and aims, *Journal of Geodynamics*, 33, 3-20.
- Rybakov, R., M.V. Goldshmidt, L. Fleischer, and Y. Rotstein (2001), Cave detection and 4-D monitoring: A microgravity case history near the Dead Sea, *The Leading Edge*, 20, 896-900.
- Rybakov, M., Y. Rotstein, B. Shirman, A. Alzaubi (2005), Cave detection near the dead sea- a micromagnetic feasibility study, *The Leading Edge*, 24, 585-590.
- Santos, F.A.M., and A. R.A. Afonso (2005), Detection and 2d modeling of cavities using pole-dipole array, *Environmental Geology*, 48, 108-116; DOI 10.1007/s00254-005-1272-8.
- Schmidt, P. W., and D.A. Clark (2006), The magnetic gradient tensor: Its properties and uses in source characterization, *The Leading Edge*, 24, 75-78.
- Spiegel, R.J., V.R. Sturdivant, and T.E. Oven (1980), Modeling resistivity anomalies from localized voids under irregular terrain, *Geophysics*, 45, No 7, p.1164-1183.
- Styles, P., R. McGrath, E. Thomas, N.J. Cassidy (2005), The use of microgravity for cavity characterization in karstic terrains, *Quarterly Journal of Engineering Geology and Hydrology*, 38, 155-169.
- Takahashi, K. (2006), Detection and localization of subsurface objects by ground penetrating radar, PhD Dissertation, Tohoku University, Japan.
- Torge, W. (2001), *Geodesy*, De Gruyter, 3rd edition, Berlin.
- Telford, W.M., L.P. Geldart, R.E. Sheriff, and D.A. Keys (1976), *Applied Geophysics*, Cambridge U. Press, New York.
- Van Der Hilst, R. (2004), *Essentials of Geophysics*, MIT-OCW, Lecture notes (<http://ocw.mit.edu>).
- Witten A. J. (2006), *Handbook of Geophysics and Archeology*, Equinox, London.

Xia, J., J.E. Nyquist, Y. Xu, M.J.S. Roth, R. D. Miller (2007), Feasibility of detecting near surface feature with Rayleigh wave diffraction, *Journal of Applied Geophysics*, 62, p. 244-253, doi: 10.1016/j.jappgeo.2006.12.002.

Zhdanov M.S., and G.V. Keller (1994), *The Geoelectrical Methods in Geophysical Exploration*, Elsevier, Amsterdam.

Zhou, W., B.F. Beck, A.L. Adams (2002), Effective electrode array in mapping karst hazards in electrical resistivity tomography, *Environmental Geology*, 42, 922-928.

Appendix A:

The Laplacian of the reciprocal distance is given by:

$$\nabla^2\left(\frac{1}{r}\right) = \left(\frac{\partial^2}{\partial x^2} + \frac{\partial^2}{\partial y^2} + \frac{\partial^2}{\partial z^2}\right)\left(\frac{1}{r}\right) \quad (\text{A.1})$$

$$\text{where } r^2 = x^2 + y^2 + z^2. \quad (\text{A.2})$$

The following derivatives are obtained by applying the general principles of differentiation:

$$\left(\frac{1}{(u^2 + a)^{1/2}}\right)'' = \left(-\frac{u}{(u^2 + a)^{3/2}}\right)' = \frac{2u^2 - a}{(u^2 + a)^{5/2}} \quad (\text{A.3})$$

If we apply the following substitutions in the expression for r in (A.1)

$$\begin{aligned} y^2 + z^2 &\rightarrow a \\ x^2 + z^2 &\rightarrow b \\ x^2 + y^2 &\rightarrow c \end{aligned} \quad (\text{A.4})$$

and use (A.3), we obtain the following for (A.1):

$$\nabla^2\left(\frac{1}{r}\right) = \left(\frac{2x^2 - a}{(x^2 + a)^{5/2}} + \frac{2y^2 - b}{(y^2 + b)^{5/2}} + \frac{2z^2 - c}{(z^2 + c)^{5/2}}\right) = \left(\frac{2r^2 - 2r^2}{r^5}\right) = 0 \quad (\text{A.5})$$

However this is true only if $r \neq 0$. How does (A.1) behave for $r \rightarrow 0$?

To understand the behavior of (A.1) as $r \rightarrow 0$, let us define a parameter ε , and make the substitution $\frac{1}{r} \rightarrow \frac{1}{\sqrt{r^2 + \varepsilon^2}}$. We seek to see the behavior of (A.1) as $\varepsilon \rightarrow 0$.

If the substitutions (A.4) are replaced by

$$\begin{aligned} a &\rightarrow y^2 + z^2 + \varepsilon^2 \\ b &\rightarrow x^2 + z^2 + \varepsilon^2 \\ c &\rightarrow x^2 + y^2 + \varepsilon^2 \end{aligned} \quad (\text{A.6})$$

and the same procedure of differentiation (as in the derivation of A.5) is followed, one obtains

$$\nabla^2\left(\frac{1}{\sqrt{r^2 + \varepsilon^2}}\right) = -\frac{3\varepsilon^2}{(r^2 + \varepsilon^2)^{5/2}} \quad (\text{A.7})$$

In order to analyze the behavior of (A.7) as $\varepsilon \rightarrow 0$, let's define a function

$$f(r, \varepsilon) = \frac{1}{4\pi} \frac{3\varepsilon^2}{(r^2 + \varepsilon^2)^{5/2}} \quad (\text{A.8})$$

We will seek the behavior of $f(r, \varepsilon)$ as $\varepsilon \rightarrow 0$. If we integrate $f(r, \varepsilon)$ over a solid sphere (a ball) of radius a :

$$\int_v f(r, \varepsilon) dv = 4\pi \int_{r < a} \frac{1}{4\pi} \frac{3\varepsilon^2 r^2 dr}{(r^2 + \varepsilon^2)^{5/2}} = \frac{a^3}{(a^2 + \varepsilon^2)^{3/2}} \quad (\text{A.9})$$

Instead of a sphere consider an arbitrary volume, D , that contain the point $r=0$. Divide this volume into two parts; a sphere Ω entirely within D and centered at $r=0$, and the region $D-\Omega$. Within $D-\Omega$, the function $f(r, \varepsilon)$ is zero for $\varepsilon^2=0$ since $r \neq 0$, hence the integral over $D-\Omega$ is zero in the limit. Within Ω , the integral approaches unity as $\varepsilon^2 \rightarrow 0$. Then, we can summarize the integral of $f(r, \varepsilon)$ (A.9) for $\varepsilon \rightarrow 0$ as follows:

$$\lim_{\varepsilon \rightarrow 0} \int_D f(r, \varepsilon) dv = \begin{cases} 1 & r = 0 \text{ inside } D \\ 0 & r = 0 \text{ outside } D \end{cases} \quad (\text{A.10})$$

Let's define a bounded function $F(x, y, z)$ which is continuous at the origin; and consider the following integral for $\varepsilon \rightarrow 0$:

$$\lim_{\varepsilon \rightarrow 0} \int_D F(x, y, z) f(r, \varepsilon) dv \quad (\text{A.11})$$

We immediately see that the integral will vanish in the limit, $\varepsilon \rightarrow 0$, if D does not contain the origin, by the previous reason. If the origin is inside D , this region can be replaced by a small sphere centered at the origin, where F is by definition still continuous. Within this sphere one can write

$$F(0,0,0) - \eta < F(x, y, z) < F(0,0,0) + \eta, \quad (\text{A.12})$$

where the number η can be made as small as desired if the sphere is made sufficiently small. We can easily see that in the limit, $\varepsilon \rightarrow 0$, $F(x, y, z)$ can be assigned its value $F(0,0,0)$ and removed from the integrand in (A.11). Then the integrand will consist of $f(r, \varepsilon)$ whose integral is known to be unity, from (A.10). Consequently (A.11) can be written as

$$\lim_{\varepsilon \rightarrow 0} \int_D F(x, y, z) f(r, \varepsilon) dv = \begin{cases} F(0,0,0) & r = 0 \text{ inside } D \\ 0 & r = 0 \text{ outside } D \end{cases} \quad (\text{A.13})$$

Instead of writing the integrals (A.10) and (A.13) in limiting forms, we introduce the *Dirac delta function* as

$$\lim_{\varepsilon \rightarrow 0} \int_D f(r, \varepsilon) dv = \int_D \delta(x, y, z) dv \quad (\text{A.14})$$

or simply as

$$\lim_{\varepsilon \rightarrow 0} f(r, \varepsilon) = \delta(r) \quad (\text{A.15})$$

and

$$\int_D F(x, y, z) \delta(r) dv = F(0, 0, 0) \quad (\text{A.16})$$

Returning back to solution (A.7), it can be also be rewritten using (A.8) as

$$\nabla^2 \left(\frac{1}{\sqrt{r^2 + \varepsilon^2}} \right) = -4\pi f(r, \varepsilon) \quad (\text{A.17})$$

For the limiting case of $\varepsilon \rightarrow 0$, the function $f(r, \varepsilon)$ in (A.17) can be replaced by the Dirac delta function using (A.15):

$$\nabla^2 \left(\frac{1}{r} \right) = -4\pi \delta(r) \quad (\text{A.18})$$

A general definition of *the Dirac delta function* can be made by expanding the arbitrary volume D into the entire space in (A.10) and (A.13): Then the following two equations completely define the Dirac delta function in three-dimensional space:

$$\int_{\infty} \delta(r) dv = 1 \quad (\text{A.19})$$

And

$$\int_{\infty} F(x, y, z) \delta(r) dv = F(0, 0, 0) \quad (\text{A.20})$$